



Linking biogeochemistry to hydro-geometrical variability in tidal estuaries: a generic modeling approach

Chiara Volta¹, Goulven Gildas Laruelle¹, Sandra Arndt², and Pierre Regnier¹

¹Department of Geoscience, Environment & Society, Université Libre de Bruxelles, Brussels, Belgium

²School of Geographical Sciences, University of Bristol, Bristol, UK

Correspondence to: Chiara Volta (cvolta@ulb.ac.be)

Received: 2 June 2015 – Published in Hydrol. Earth Syst. Sci. Discuss.: 1 July 2015

Accepted: 9 February 2016 – Published: 7 March 2016

Abstract. This study applies the Carbon-Generic Estuary Model (C-GEM) modeling platform to simulate the estuarine biogeochemical dynamics – in particular the air–water CO₂ exchange – in three idealized tidal estuaries characterized by increasing riverine influence, from a so-called “marine estuary” to a “riverine estuary”. An intermediate case called “mixed estuary” is also considered. C-GEM uses a generic biogeochemical reaction network and a unique set of model parameters extracted from a comprehensive literature survey to perform steady-state simulations representing average conditions for temperate estuaries worldwide. Climate and boundary conditions are extracted from published global databases (e.g., World Ocean Atlas, GLORICH) and catchment model outputs (GlobalNEWS2). The whole-system biogeochemical indicators net ecosystem metabolism (NEM), C and N filtering capacities (FC_{TC} and FC_{TN}, respectively) and CO₂ gas exchanges (FCO₂) are calculated across the three idealized systems and are related to their main hydrodynamic and transport characteristics. A sensitivity analysis, which propagates the parameter uncertainties, is also carried out, followed by projections of changes in the biogeochemical indicators for the year 2050.

Results show that the average C filtering capacities for baseline conditions are 40, 30 and 22 % for the marine, mixed and riverine estuary, respectively, while N filtering capacities, calculated in a similar fashion, range from 22 % for the marine estuary to 18 and 15 % for the mixed and the riverine estuaries. Sensitivity analysis performed by varying the rate constants for aerobic degradation, denitrification and nitrification over the range of values reported in the literature significantly widens these ranges for both C and N. Simulations for the year 2050 suggest that all estuaries will remain

largely heterotrophic, although a slight improvement of the estuarine trophic status is predicted. In addition, our results suggest that, while the riverine and mixed systems will only marginally be affected by an increase in atmospheric *p*CO₂, the marine estuary is likely to become a significant CO₂ sink in its downstream section. In the decades to come, such a change in behavior might strengthen the overall CO₂ sink of the estuary–coastal ocean continuum.

1 Introduction

Located at the interface between land and ocean, estuaries are highly dynamic ecosystems, which process variable fractions of land-derived inputs of carbon (C) and nutrients (N, P, Si) through a wide range of chemical and biological processes (Alongi, 1998; Crossland et al., 2005; Bianchi, 2007). Gaseous species, in particular CO₂, are produced and further exchanged with the atmosphere as a result of these intense biogeochemical dynamics. Recent compilations of observed data reveal that the vast majority of estuarine systems are net CO₂ emitters (Laruelle et al., 2010, 2013; Borges and Abril, 2011) and are responsible for a global CO₂ outgassing ranging between 0.15 and 0.25 PgC yr^{−1} (Cai, 2011; Bauer et al., 2013; Regnier et al., 2013a). This flux corresponds to about 20–25 % of the riverine carbon inputs and is of similar magnitude to the global uptake of CO₂ by continental shelves (Laruelle et al., 2014). Estuaries are thus important modulators of the carbon and associated bio-elements fluxes from the land to the open ocean (e.g., Jahnke, 1996; Billen and Garnier, 1997; Gattuso et al., 1998; Lancelot et al., 2005; Mackenzie et al., 2005; Arndt et al., 2009, 2011a; Laru-

elle et al., 2009; Borges and Abril, 2011; Cai, 2011; Bauer et al., 2013; Regnier et al., 2013a). However, the extent to which their biogeochemical dynamics and thus their role in the global cycles will change in the future in response to anthropogenically driven changes in land use, climate and atmospheric CO₂ remains poorly known.

Over the past 30 years, highly resolved, process-oriented and often multi-dimensional models have helped disentangle and quantify estuarine biogeochemical dynamics (e.g., Thomann and Fitzpatrick, 1982; Lung and Paerl, 1988; Regnier et al., 1997, 1999; Margvelashvili et al., 2003; Baklouti et al., 2011; Cerco, 2000; Arndt et al., 2007, 2009; Mateus et al., 2012). Most of these studies have focused on specific estuarine systems, and comparative studies covering the wide range of estuarine systems are limited. Therefore, a quantitative evaluation of the role of estuaries in the global biogeochemical cycles and their potential response to global change are characterized by large uncertainties (Hobbie, 2000; Borges and Abril, 2011; Laruelle et al., 2013; Regnier et al., 2013a). This lack can be partly attributed to the high data requirements for model calibration and validation, as well as the high computational demand, which have prevented their application to regional and/or global scales (Bauer et al., 2013). In addition, the limited availability of comparative studies compromises the identification of common patterns across the wide range of estuarine types (Geyer et al., 2000; Hobbie, 2000; Borges and Abril, 2011; Regnier et al., 2013b). Moreover, the diagnostic modeling of the CO₂ dynamics has so far only been performed for a temperate estuary in Europe (the Scheldt; Vanderborgh et al., 2002), although observational data are now available for more than 100 land–ocean transition systems (Chen et al., 2013; Laruelle et al., 2013). To our knowledge, prognostic simulations of greenhouse gas emissions in estuaries are currently lacking.

The objectives of this paper are thus to develop a unified modeling approach to identify similarities and differences in the biogeochemical dynamics across different estuarine systems and to explore quantitative relationships between the estuarine biogeochemical functioning and a set of key hydro-geometrical characteristics. The overarching goal is to enhance our ability to transfer information from well-constrained estuarine systems to poorly surveyed systems, to improve upscaling strategies and to enable projections. In the first part of this paper, the description of the conceptual framework underlying our generic approach is provided. In particular, we build on the mutual dependency between geometry and hydrodynamics (Savenije, 1992, 2005, 2012) and further hypothesize that hydrodynamics exert a strong control on biogeochemistry in alluvial estuaries (e.g., Alpine and Cloern, 1992; Arndt et al., 2007; Volta et al., 2014). Next, three idealized systems, characterized by variable riverine influence and covering the main hydro-geometrical features of tidal alluvial estuaries, are modeled using the recently developed C-GEM modeling platform (Volta et al., 2014). These

systems are designed to represent a tidal estuary dominated by marine characteristics, a tidal estuary dominated by its riverine characteristics, and an intermediate case (so-called mixed system). Here, C-GEM uses a generic biogeochemical reaction network and a unique parameter set extracted from a large literature survey of more than 40 local modeling studies. Steady-state simulations representing average conditions for temperate estuaries worldwide are performed for the present decade, as well as for the mid-21st century. The whole-system biogeochemical indicators net ecosystem metabolism (NEM), C and N filtering capacities (FC_{TC} and FC_{TN}, respectively) and CO₂ gas exchanges (FCO₂) are calculated across the three idealized systems and are related to their main hydrodynamic and transport characteristics. A sensitivity analysis is also carried out to assess the sensitivity of the estuarine biogeochemical functioning to parameter uncertainties synthesized in the present study. Finally, the main findings are summarized and their significance and limitations are critically analyzed in the context of improving up-scaling strategies for regional and global CO₂ emissions of estuaries.

2 Description of modeling approach

2.1 Theoretical support

Most tidal estuaries are alluvial estuaries (Regnier et al., 2013b), which are defined as estuarine systems with movable beds, consisting of material from marine and terrestrial origin, and a measurable freshwater inflow (e.g., Hobbie, 2000; Savenije, 2005, 2012). The global distribution of alluvial estuaries is roughly equivalent to that of the tidal estuaries as defined in the estuarine coastal typology of Dürr et al. (2011). The approach developed here builds on this intercompatibility, already mentioned in Regnier et al. (2013b). In tidal estuaries, two different zones can be identified along their longitudinal gradient: a lower zone, the so-called saline estuary, whose dynamics are essentially controlled by mixing with marine waters, and an upstream zone, referred to as the tidal river, where processes are mainly driven by the freshwater input from rivers (e.g., Jay et al., 1990; Dalrymple et al., 1992; Regnier et al., 2013b). Alluvial estuaries are characterized by a mutual dependency of the estuarine geometry and hydrodynamics. The magnitude of the water flow entering or leaving the estuarine channel is entirely controlled by its shape (Pethick, 1984). In turn, the water movement, mainly driven by tides and freshwater discharge, leads to a redistribution of the unconsolidated sediments that determines the shape of the estuary. This dynamic interplay between hydrodynamics and morphology results in a continuum of estuarine shapes that cover the entire spectrum between two end-member cases: (1) systems with rapidly converging banks towards the land and (2) systems characterized by parallel banks (Savenije, 1992). Although the exact shape

of alluvial estuaries can vary, they nonetheless show common geometrical characteristics that are compatible with an idealized representation of the estuarine geometry (Savenije, 2005, 2012). The tidally averaged estuarine width \bar{B} (in m) typically shows an exponential decrease in the landward direction (e.g., Pethick, 1992; Lanzoni and Seminara, 1998; Savenije, 1992, 2005), while the tidally averaged estuarine depth \bar{H} (in m) remains nearly constant along the estuarine gradient (Savenije, 1992, 2005, 2012):

$$\bar{B}(x) = B_0 \cdot \exp\left(-\frac{x}{b}\right), \quad (1)$$

$$\bar{H}(x) = H_0, \quad (2)$$

where x (in m) is the distance from the estuarine mouth, B_0 and H_0 denote the estuarine width and depth (in m) at the estuarine mouth ($x = 0$), respectively, and b is the width convergence length (in m), defined as the distance over which the estuarine width reduces to 37 % (e^{-1}) of its value at the mouth. The shape of alluvial estuaries can, thus, be fully defined by the width convergence length, b , and the channel depth, H_0 (Savenije, 2012). The ratio between these two geometrical key parameters is generally defined as the dimensionless estuarine shape number, S (Savenije, 1992):

$$S = \left(\frac{b}{H_0}\right). \quad (3)$$

The hydrodynamic characteristics of alluvial estuaries may, in turn, be directly related to their main hydrodynamic forcings, such as tidal influence and freshwater inflow (Wright et al., 1973) by means of the dimensionless hydrodynamic Canter–Cremers estuary number N (Simmons, 1955):

$$N = \frac{Q_b \cdot T}{P} \approx \frac{Q_b \cdot T}{A_0 \cdot E}, \quad (4)$$

where Q_b denotes the bankfull discharge or, in other words, the temporary maximum river discharge (in $\text{m}^3 \text{s}^{-1}$) that is associated with a state of maximum flow velocity and, thus, to the maximum ability to shape the estuary (Savenije, 2012). T is the tidal period (in s). P is the tidal prism (in m^3), which represents the volume of saline water entering the estuary over a tidal period, T , and can be approximated by the product of the cross-sectional area at the estuarine mouth A_0 (in m^2) ($A_0 = B_0 \cdot H_0$) and the tidal excursion length E (in m), defined as the maximum distance a water particle travels during a tidal period T . By using a regression analysis based on measurements from 16 alluvial estuaries worldwide, Savenije (1992) showed that the estuarine shape number (S ; Eq. 3) is related to the hydrodynamic Canter–Cremers number (N ; Eq. 4) through a power law relationship, resulting in the dimensionless hydro-geometrical relationship:

$$\frac{b}{H_0} = 12\,500 \cdot \left(\frac{Q_b \cdot T}{A_0 \cdot E}\right)^{0.26}. \quad (5)$$

Certain hydro-geometrical characteristics, such as the tidal period T , the tidal excursion E and the estuarine depth at the mouth H_0 can be approximated by characteristic values. For instance, E is usually close to 10 km for a semi-diurnal ($T \approx 12$ h) tidal estuary, while an alluvial estuary flowing in a coastal plain generally reveals a tidally averaged depth (\bar{H}) of about 7 m (Savenije, 1992; Volta et al., 2014). Note that, for estuaries in which the freshwater discharge is known, a new formulation proposed by Gisen and Savenije (2015) can be used to estimate the estuarine depth. On the other hand, other characteristics, such as the bankfull discharge Q_b , the width convergence length b , and the cross-sectional area at the estuarine mouth A_0 , are system-specific characteristics, depending on the hydrological regime of the estuarine watershed and on the local balance between riverine and marine energies. Therefore, they cannot be easily approximated. The width convergence length, b , and the bankfull riverine discharge, Q_b , can thus be considered key parameters for defining the hydro-geometrical character of alluvial estuaries and for predicting their salt intrusion profiles (Savenije, 2005, 2012). Important transport and mixing properties can be directly related to these hydro-geometrical characteristics. Hence, Eq. (5) not only provides a universal theoretical framework for analyzing the tight link between geometry, hydrodynamics and transport but also offers a theoretical basis for a classification of alluvial estuaries. Savenije (2005, 2012) identified two main estuarine types, which differ in terms of geometrical features, hydrodynamics characteristics and salt intrusion patterns:

1. funnel-shaped (or marine-dominated) estuaries that are typically characterized by a short width convergence length, b , and thus rapidly converging banks, a low freshwater discharge, a dome-shaped salinity profile with a small salinity gradient at the estuarine mouth and an intrusion of saltwater far upstream;
2. prismatic (or river-dominated) estuaries that are characterized by a theoretically infinite width convergence length, b , and, thus, a constant channel width, a high river discharge and a steep salt intrusion profile with a strong salinity gradient close to the estuary mouth and a short salt intrusion length.

These estuarine classes represent the extreme ends of the wide range of estuarine hydro-geometrical properties. As a consequence, a series of systems, which show intermediate conditions and fall in between the funnel-shaped and the prismatic end-member cases, can be hypothesized between them (Savenije, 1992). Physical and hydrodynamic characteristics as they relate to the estuary shape are synthesized in Fig. 1 by specifying how they behave in a predominantly funnel-shaped or prismatic estuary and by reporting real-world estuaries as examples.

The identification of two end-member estuarine classes and an intermediate group, on the one hand, and the recog-

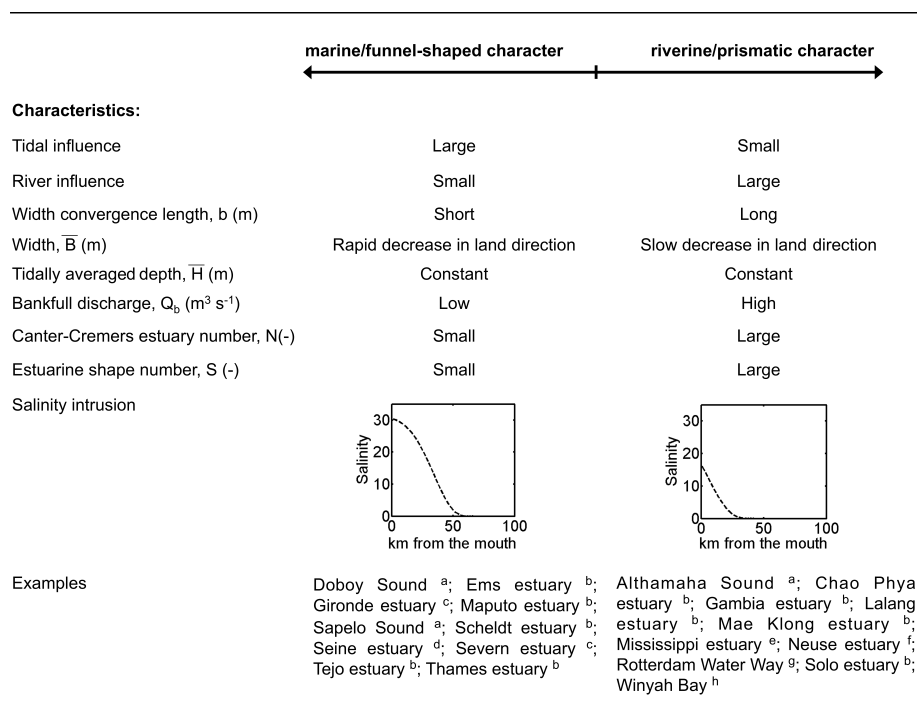


Figure 1. Relationships between morphological and hydrodynamical factors in alluvial estuaries. Examples refer to real-world estuaries typically reported as marine- and riverine-dominated systems in the estuarine research: ^a Jiang et al. (2008), ^b Savenije (1992), ^c Wells (1995), ^d Dauvin et al. (2008), ^e Pritchard (1967), ^f Gaulke et al. (2010), ^g Toffolon et al. (2006), ^h Goñi et al. (2003).

dition of the first-order control of hydrodynamics on estuarine biogeochemistry (e.g., Alpine and Cloern, 1992; Nixon et al., 1996; Arndt et al., 2007, 2009; Laruelle et al., 2009), on the other hand, allow hypothesizing that each estuarine type might respond in a specific way to the tight coupling between geometry, hydrodynamics, transport and biogeochemistry. Hence, important biogeochemical properties in estuaries might, just as salinity profiles, be predicted on the basis of hydro-geometrical features (Fig. 2; Volta et al., 2014).

2.2 Representative estuarine systems

In this study, we explore the link between biogeochemical dynamics and key hydro-geometrical properties in three idealized, tidal alluvial estuaries characterized by variable marine/riverine influence by means of a reactive-transport model. For this purpose, three idealized geometries are defined to be representative of the two extreme classes and the intermediate types as described in Sect. 2.1 (marine- and riverine-dominated estuaries and intermediate cases). The width convergence length, b , recognized as a shape and hydrodynamic key parameter (see Sect. 2.1), is used to discriminate between the three estuarine types. First, a reference estuary, characterized by an idealized geometry resembling that tested in Volta et al. (2014), is defined. Then, its width convergence length ($b = 30$ km) is decreased and increased by 50 % in order to intensify the marine ($b = 15$ km)

and the riverine ($b = 45$ km) character of the system, respectively. This allows defining two other idealized systems, which can be regarded as representative of the marine and river-dominated estuarine classes and between which the reference estuary can be considered an intermediate case. Henceforth, according to Regnier et al. (2013b) and Volta et al. (2014), the marine-dominated estuary, the reference case and the riverine-dominated estuary will be referred to as the marine, the mixed and the riverine estuary, respectively. The estuarine width at the seaward limit, B_0 , and the estuarine length, EL , of the marine and the riverine estuaries are adjusted so that their total, tidally averaged volume corresponds to that of the mixed estuary ($\bar{V} \approx 1.5 \times 10^9 \text{ m}^3$). This allows minimizing the effect of volume variations on the biogeochemical dynamics across the three estuarine types. As a result, the channel width of the marine-dominated estuary reduces, over a distance of 90 km, from 13 830 m at the estuarine mouth to 30 m close to the upper limit, whereas the width of the riverine-dominated estuary decreases, over a distance of 226 km, from 4760 m at the estuary mouth to 30 m at the upper limit. All estuaries are assumed to be coastal plain estuaries. Hence, their tidally averaged water depth is approximated to 7 m (see Sect. 2.1). Furthermore, it is assumed that the three idealized systems are subject to a semi-diurnal tidal forcing, thus resulting in an identical tidal excursion length, E , of approximately 10 km (see Sect. 2.1). Based on these geometrical characteristics, Eq. (5) can be

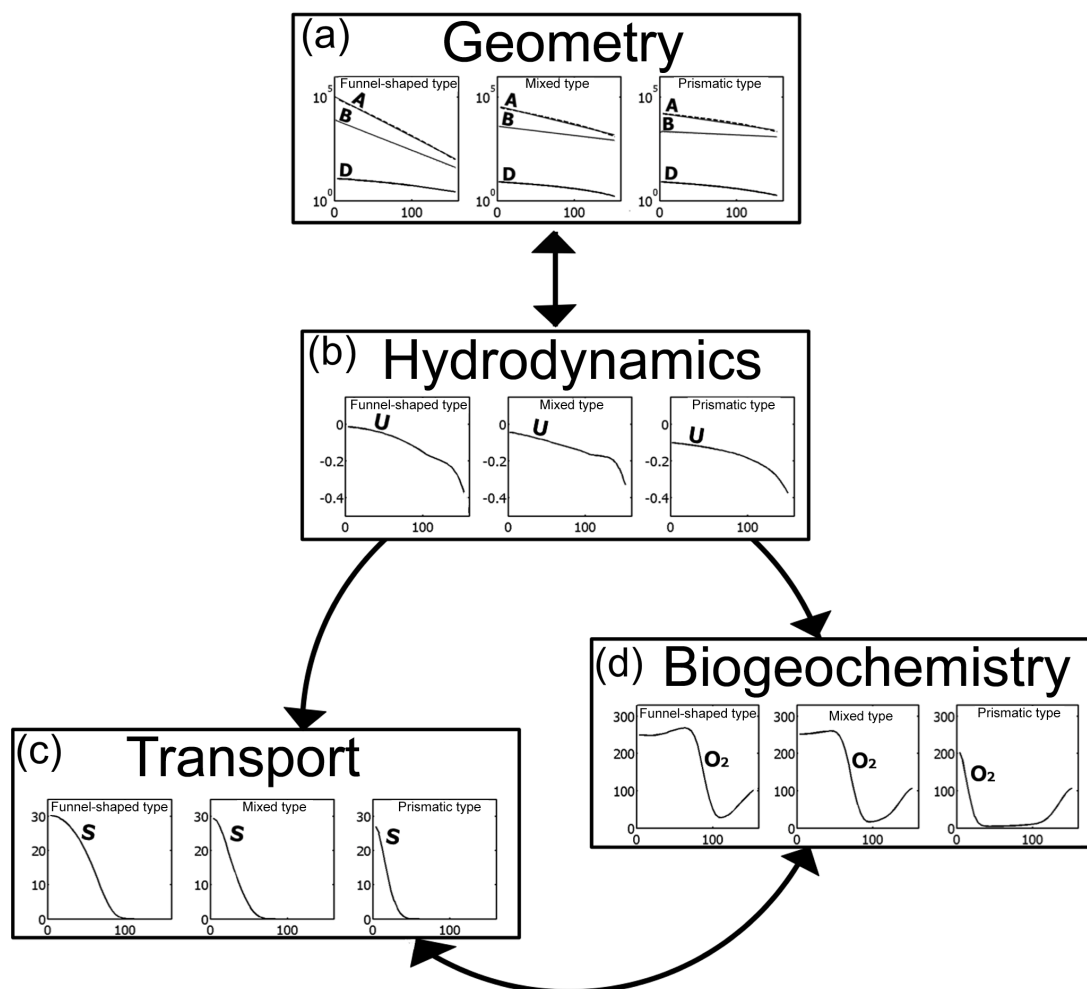


Figure 2. Conceptual scheme of the generic modeling approach (from Volta et al., 2014). Each estuarine type responds in a specific manner to the interdependence between geometry and hydrodynamics and to the first-order control of the hydrodynamics on transport and biogeochemistry. Small panels correspond to longitudinal distribution of (a) A (cross-section area, in m^2), B (width, in m), and H (depth, in m); (b) water flow velocity (in m s^{-1}); (c) salinity; and (d) O_2 concentration (in $\mu\text{M O}_2$).

used to calculate the bankfull discharge, Q_b in $\text{m}^3 \text{s}^{-1}$, for each system. New formulations are now available to constrain the bankfull discharge from geometrical parameters (i.e., depth and width; see Gisen and Savenije, 2015) and they could be used in future applications of C-GEM. The geometrical features of the three idealized estuaries are illustrated in Fig. 3 and summarized, together with their hydrodynamic properties, in Table 1. Table 1 also reveals that both the estuarine shape (S , Eq. 3) and the hydrodynamic Canter–Cremers (N , Eq. 4) numbers of the three idealized systems cover the whole range of observed values for temperate tidal estuaries ($2500 < S < 6000$, $N < 0.05$; Savenije, 1992). As a consequence, they may be considered as representative of a large range of hydro-geometrical conditions observed in this type of estuaries. Note that higher values of S have been reported for tropical estuaries (Gisen et al., 2015).

2.3 Model description

Simulations presented in this study are performed by using the C-GEM modeling platform, fully described and available as supplementary material in Volta et al. (2014). C-GEM dynamically resolves hydrodynamics, transport and pelagic biogeochemistry using the numerical schemes described in Regnier and Steefel (1999) and explicitly accounts for variations induced by tides. Here, we use a version of C-GEM similar to that described in Volta et al. (2014), but its biogeochemical reaction network was extended to include a non-siliceous phytoplanktonic group and an inorganic carbon module.

Table 1. Geometrical and hydrodynamic parameters describing the three idealized estuaries. Following Eq. (2), $H_0 = \bar{H}$ for alluvial estuaries flowing in a coastal plain. \bar{V} is the total estuarine volume calculated as $\bar{V} = \int_0^{\text{EL}} [(\bar{H}(x) + \zeta(x)) \cdot B(x)] dx$.

Name	Description	Value		
		Marine estuary	Mixed estuary	Riverine estuary
EL	Estuarine length [km]	90	160	226
H_0	Depth at the estuarine mouth [m]	7	7	7
B_0	Width at the estuarine mouth [m]	13 830	7100	4760
B_x	Width at the estuarine upper limit [m]	30	30	30
A_0	Cross-sectional area at the estuarine mouth [m ²]	96 810	49 700	33 320
\bar{V}	Total tidally averaged estuarine volume [km ³]	1.548	1.535	1.524
b	Width convergence length [m]	15 000	30 000	45 000
T	Tidal period [s]	45 720	45 720	45 720
E	Tidal excursion [m]	10 000	10 000	10 000
P	Tidal prism [km ³]	1.38	0.71	0.48
ζ_0	Tidal amplitude at the estuarine mouth [m]	3.5	3.5	3.5
Q_b	Bankfull freshwater discharge [m ³ s ⁻¹]	24	177	565
S	Estuarine shape number [–]	2143	4286	6429
N	Canter–Cremers estuary number [–]	8.0×10^{-4}	1.1×10^{-2}	5.4×10^{-2}

2.3.1 Physical model support and hydrodynamic module

The three idealized hydro-geometrical estuarine cases, as described in Sect. 2.2, form the physical support and provide the boundary conditions for the hydrodynamic module of C-GEM. The latter resolves the cross-sectionally integrated mass and momentum conservation equations for a channel with arbitrary geometry (Nihoul and Ronday, 1976; Regnier et al., 1998; Regnier and Steefel, 1999):

$$r_s \frac{\partial A}{\partial t} + \frac{\partial Q}{\partial x} = 0, \quad (6)$$

$$\frac{\partial U}{\partial t} + U \frac{\partial U}{\partial x} = -g \frac{\partial \zeta}{\partial x} - g \frac{U|U|}{C_h^2 H}, \quad (7)$$

where t is the time (in s); x is the space (in m); r_s is the dimensionless storage water ratio that is typically equal to 1 for idealized representations of estuarine geometries (Davies and Woodroffe, 2010); A is the cross-sectional area (in m²), calculated by the product of the estuarine width B , formulated as in Eq. 1, and the instantaneous water depth H , computed as the sum of the tidally averaged water depth (in m) and the water elevation $\zeta(x, t)$ (in m); Q is the cross-sectional discharge (in m³ s⁻¹), calculated by the product of A (in m²) and the flow velocity U (in m s⁻¹); g is the gravitational acceleration (in m s⁻²); and C_h is the Chézy coefficient (in m^{1/2} s⁻¹).

2.3.2 Coupling reaction and transport

The coupling of mass transport and chemical reactions is described by using a one-dimensional, tidally resolved advection–dispersion equation for gaseous, solute and solid species in the water column (e.g., Pritchard, 1958):

$$\frac{\partial C_i}{\partial t} + \frac{Q}{A} \frac{\partial C_i}{\partial x} = \frac{1}{A} \frac{\partial}{\partial x} \left(AD \frac{\partial C_i}{\partial x} \right) + P_i, \quad (8)$$

where C_i is the concentration of the species i , A is the cross-sectional area (in m²) and D is the dispersion coefficient (in m² s⁻¹), which decreases in the upstream direction according to the Van der Burgh equation (Savenije, 1986) and is dynamically calculated as in Volta et al. (2014). Finally, P_i is the sum of volumetric biogeochemical reactions and exchanges through the material surfaces of the estuary (e.g., gas transfer through the air–water interface, erosion and deposition processes), affecting species i . The transport and reaction terms are solved in sequence by applying the operator-splitting approach proposed by Regnier et al. (1998) and a finite-difference scheme on a regular grid ($\Delta x = 2000$ m) with a time step $\Delta t = 150$ s. In the transport equation, the dispersive and the advective terms are solved by using the semi-implicit Crank–Nicolson algorithm (Press et al., 1992) and the third-order Leonard total variation diminishing scheme (Leonard, 1984; Datta-Gupta et al., 1991), respectively. These schemes guarantee mass conservation to within $> 1\%$. Reaction processes are numerically integrated using the Euler method (Press et al., 1992). A spin-up period of 24 months is imposed.

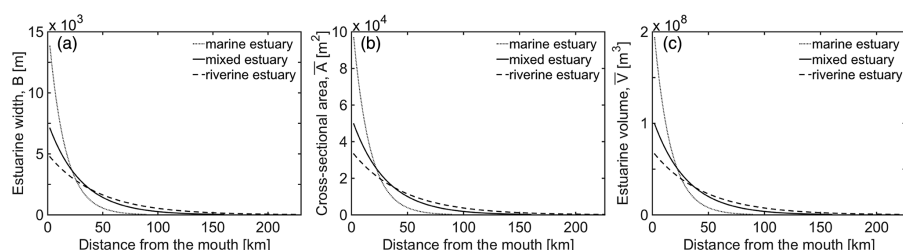


Figure 3. Variability along the estuarine axis of (a) width B (m), (b) cross-sectional area \bar{A} (m^2) and (c) volume \bar{V} (m^3) in the three idealized estuaries. Note that the estuarine length EL (km) varies across systems. \bar{A} is calculated as the product of the tidally averaged depth \bar{H} ($\bar{H} = 7$ m along EL) and B and \bar{V} is the product between \bar{A} and Δx . Profiles are obtained by using geometrical parameters reported in Table 1.

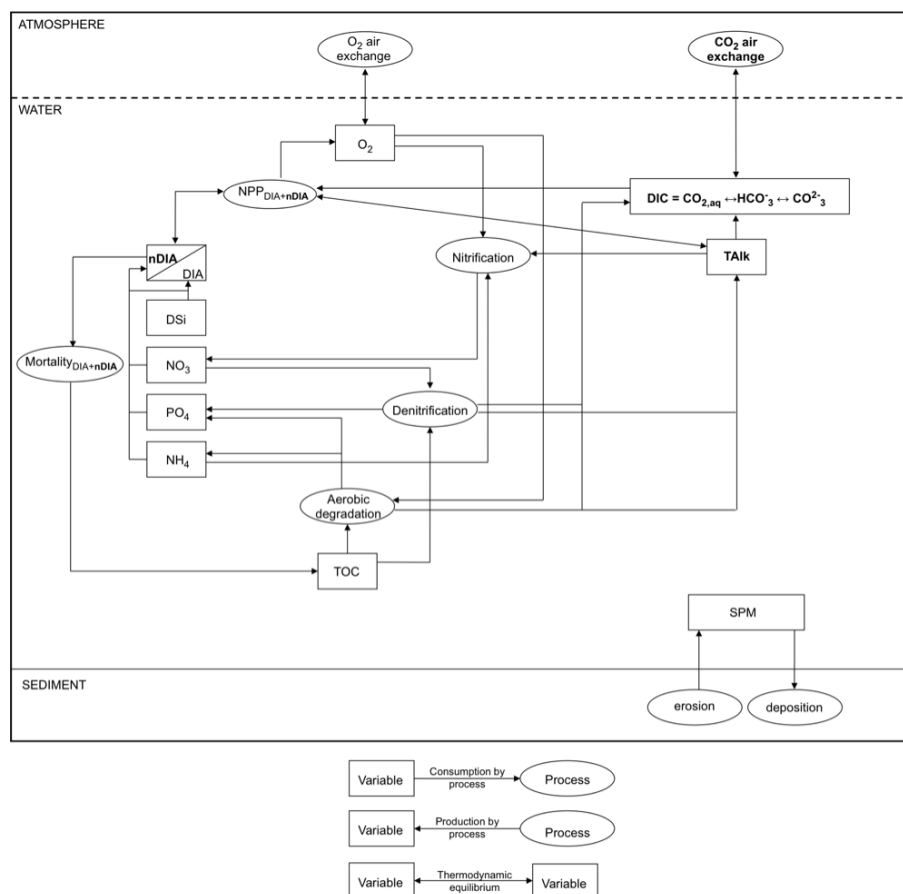


Figure 4. Conceptual scheme of the C-GEM reaction network as implemented in this study. The new variables and reactions compared to the version presented in Volta et al. (2014) are highlighted in bold.

2.3.3 Reaction network

The reaction network of C-GEM includes 12 state variables and 10 biogeochemical processes (Table 2). Table 3 summarizes the stoichiometric equation and mathematical formulation of each biogeochemical reaction, while the biogeochemical scheme of the reaction module is shown in Fig. 4. The original version C-GEM 1.0 is described in detail in Volta et al. (2014). Here, it is extended by a second phytoplankton

group (nDIA), which represents non-siliceous phytoplanktonic species, such as cyanobacteria, green algae and flagellates, whose growth does not depend on silica concentrations. Furthermore, a new inorganic carbon module, which allows quantifying the estuarine inorganic carbon dynamics, was also implemented. Its mathematical formulation is adapted from Arndt et al. (2011b). pH is considered the master variable for the estimation of dissolution and hydration of CO_2 and is calculated by using the computationally fast approach

Table 2. State variables and processes explicitly implemented in C-GEM.

Name	Symbol	Unit
State variables		
Salinity	S	–
Diatoms	DIA	$\mu\text{M C}$
Non-diatom phytoplankton	nDIA	$\mu\text{M C}$
Oxygen	O_2	$\mu\text{M O}_2$
Dissolved silica	DSi	$\mu\text{M Si}$
Total organic carbon	TOC	$\mu\text{M C}$
Ammonium	NH_4	$\mu\text{M N}$
Nitrate	NO_3	$\mu\text{M N}$
Phosphate	PO_4	$\mu\text{M P}$
Dissolved inorganic carbon	DIC	$\mu\text{M C}$
Total alkalinity	TALK	$\mu\text{M C}$
Suspended particulate matter	SPM	g L^{-1}
Biogeochemical reactions		
Gross primary production	GPP	$\mu\text{M C s}^{-1}$
Net primary production	NPP	$\mu\text{M C s}^{-1}$
Phytoplankton mortality	M	$\mu\text{M C s}^{-1}$
Aerobic degradation	R	$\mu\text{M C s}^{-1}$
Denitrification	D	$\mu\text{M C s}^{-1}$
Nitrification	N	$\mu\text{M N s}^{-1}$
O_2 exchange with the atmosphere	FO_2	$\mu\text{M O}_2 \text{ s}^{-1}$
CO_2 exchange with the atmosphere	FCO_2	$\mu\text{M C s}^{-1}$
SPM erosion	E_{SPM}	$\text{g L}^{-1} \text{ s}^{-1}$
SPM deposition	D_{SPM}	$\text{g L}^{-1} \text{ s}^{-1}$

provided by Follows et al. (2006) by means of an iterative procedure, which accounts for total (TALK) and carbonate alkalinities. While the model accounts for borate species, contributions from ammonium, fluorine, phosphate, silicate, sulfide and other minor species are neglected because their concentrations are much lower than those of carbonate species (Vanderborght et al., 2002). The apparent equilibrium constants for CO_2 solubility and dissociation of carbonic acid (HCO_3^-), bicarbonate (CO_3^{2-}), water (H_2O) and boric acid (B(OH)_4^-) vary with temperature and salinity according to equations formulated by Cai and Wang (1998) and Dickson (1990). Moreover, new generic temperature-dependent functions for different physiological processes, such as for instance microbial and phytoplankton growth and decay, are implemented in the current version of C-GEM. The implementation of these terms is informed by a large modeling literature survey and further details are provided in the following section (Sect. 3).

2.3.4 Model parameterization

Sediment parameters

The sediment (SPM) module of C-GEM (Volta et al., 2014) requires specification of six parameters (Table 4). Although assembling a generic data set for sediment parameters is beyond the scope of this study, some generic assumptions are adopted for the Chézy coefficient (C_h in $\text{m}^{1/2} \text{ s}^{-1}$) and the SPM settling velocity (w_s in mm s^{-1}). In particular, as suggested by Savenije (2001, 2012), a C_h value of 40 and $60 \text{ m}^{1/2} \text{ s}^{-1}$ is applied in the tidal river and in the saline estuary, respectively, while w_s is approximated to 1 mm s^{-1} (Winterwerp, 2002). On the other hand, sediment parameters, such as the critical shear stress for erosion and deposition (τ_{cr} in N m^{-2}) and the erosion coefficient (E_{ero} in $\text{kg m}^{-2} \text{ s}^{-1}$), are usually calibrated on the basis of local SPM observations and represent system-specific fitting parameters with a limited transferability (Volta et al., 2014). Here, we adapt values reported for an idealized, tidal alluvial estuary by Volta et al. (2014).

Biogeochemical parameters

Biogeochemical parameters and their corresponding numerical values used in the C-GEM simulations are listed in Table 5. In natural waters, the Redfield ratio C : N : Si : P, which is instrumental for estimating carbon and nutrient production/consumption rates (Table 3), can be approximated by the Redfield–Brzezinski ratio 106 : 16 : 15 : 1 (Redfield et al., 1963; Brzezinski, 1985). The background light extinction coefficient (K_{D1} in m^{-1}) and the specific light attenuation of SPM (K_{D2} in $\text{mg}^{-1} \text{ m}^{-1}$) are system-specific attributes that are generally derived from local underwater light and SPM observations (Volta et al., 2014) and they are adapted here from values reported for an idealized, tidal alluvial estuary by Volta et al. (2014). All other biogeochemical parameters ($n = 18$, identified in bold in Table 5) are derived from a comprehensive literature review of all published estuarine biogeochemical model applications in temperate regions over the last 30 years. In this study, we define temperate regions as those lying between 30 and 60° in either hemisphere. As a consequence, the generic biogeochemical parameterization provided and applied in this study should be considered representative of these zones. A more detailed description of the biogeochemical parameter review and analysis is provided in Sect. 3.

2.3.5 Climate forcings and boundary conditions

Except for the freshwater discharge, all model simulations are forced with the same set of climate and hydrological forcings, representative of the mean annual conditions in temperate regions during the 2000s (Table 6). Annually averaged values of irradiance and photoperiod are calculated by using the astronomical equation of Brock (1981), while

Table 3. Formulations of the biogeochemical and sediment processes with the corresponding stoichiometric equations as implemented in the current C-GEM reaction network. T_{abs} and T denote the absolute and the Celsius temperature, respectively. H is the instantaneous water depth. PHY is the phytoplankton concentration. If PHY = DIA, nlim also accounts for the silica limitation for the phytoplankton growth. Further details can be found in Arndt et al. (2011b) and in Volta et al. (2014). Temperature functions are deduced from ^a Garcia et al. (2010); ^b Cerco (2000), Kim and Cerco (2003), Cerco and Noel (2004); ^c Chapelle et al. (1994, 2000); ^d calibration; ^e Solidoro et al. (2005); and ^f Robson and Hamilton (2004), Zheng et al. (2004). Further details about the temperature functions are given in Sect. 3.2.

Gross primary production	$GPP = P_{\text{max}}^B(T) \cdot \text{nlim} \cdot \text{PHY} \cdot \int_H^0 1 - \exp\left(-\frac{\alpha}{P_{\text{ma}}^B(T)} \cdot I(0) \cdot \exp(-K_D \cdot H)\right) dz$
Net primary production	$NPP = \frac{GPP}{H} \cdot (1 - k_{\text{excr}}) \cdot (1 - k_{\text{growth}}) - k_{\text{maint}}(T) \cdot \text{PHY}$
Phytoplankton mortality	$M = k_{\text{mort}}(T) \cdot \text{PHY}$
Aerobic degradation	$R = k_{\text{ox}}(T) \cdot \frac{\text{TOC}}{\text{TOC} + K_{\text{TOC}}} \cdot \frac{\text{O}_2}{\text{O}_2 + K_{\text{O}_2, \text{ox}}}$
Denitrification	$D = k_{\text{denit}}(T) \cdot \frac{\text{TOC}}{\text{TOC} + K_{\text{TOC}}} \cdot \frac{\text{NO}_3}{\text{NO}_3 + K_{\text{NO}_3}} \cdot \frac{K_{\text{in}, \text{O}_2}}{\text{O}_2 + K_{\text{in}, \text{O}_2}}$
Nitrification	$N = k_{\text{nit}}(T) \cdot \frac{\text{NH}_4}{\text{NH}_4 + K_{\text{NH}_4}} \cdot \frac{\text{O}_2}{\text{O}_2 + K_{\text{O}_2, \text{nit}}}$
Oxygen air exchange	$\text{FO}_2 = \frac{vp}{H} \cdot (\text{O}_{2, \text{sat}} - \text{O}_2)$
Carbon dioxide air exchange	$\text{FCO}_2 = 0.913 \frac{vp}{H} \cdot (K_H \cdot p_{\text{CO}_2, \text{atm}} - \text{CO}_2)$
Nutrient limitation for phytoplankton growth	$\text{nlim} = \frac{\text{NO}_3 + \text{NH}_4}{\text{NO}_3 + \text{NH}_4 + K_N} \cdot \frac{\text{PO}_4}{\text{PO}_4 + K_{\text{PO}_4}}$
Switch between NH_4 and NO_3 utilization	$f_{\text{NH}_4} = \frac{\text{NH}_4}{10 + \text{NH}_4}$
Light extinction coefficient	$K_D = K_{D1} + K_{D2} \cdot \text{SPM}$
Piston velocity	$vp = k_{\text{flow}} + k_{\text{wind}}$
Current component for piston velocity	$k_{\text{flow}} = \sqrt{\frac{U \cdot D_{\text{O}_2}(T_{\text{abs}})}{H}}$
Wind component for piston velocity	$k_{\text{wind}} = \frac{1}{3.6 \times 10^5} \cdot 0.31 \cdot (U_{\text{wind}, 10\text{m}} \cdot \exp(-x))^2 \cdot \sqrt{\frac{Sc(T, S)}{660}}$
Sediment erosion	$E_{\text{SPM}} = \frac{1}{H} \cdot p_{\text{ero}} \cdot E_{\text{ero}}$
Sediment deposition	$D_{\text{SPM}} = \frac{1}{H} \cdot p_{\text{dep}} \cdot w_s \cdot \text{SPM}$
Probability for erosion	$p_{\text{ero}} = \frac{\tau_b}{\tau_{\text{cr}}} - 1$ if $\tau_{\text{cr}} \leq \tau_b$ $p_{\text{ero}} = 0$ if $\tau_{\text{cr}} > \tau_b$
Probability for deposition	$p_{\text{dep}} = 1 - \frac{\tau_b}{\tau_{\text{cr}}}$ if $\tau_{\text{cr}} \geq \tau_b$ $p_{\text{dep}} = 0$ if $\tau_{\text{cr}} < \tau_b$
Critical shear stress for erosion and deposition	$\tau_b = \frac{\rho_w \cdot g \cdot U \cdot U}{C^2}$
T dependence for $P_{\text{max}}^{B, a}$	$P_{\text{max}}^B(T) = P_{\text{max}}^B \cdot 1.067^{(T - T_{\text{ref}})}$
T dependence for k_{maint}^b	$k_{\text{maint}}(T) = k_{\text{maint}} \cdot \exp(0.0322 \cdot (T - T_{\text{ref}}))$
T dependence for k_{mort}^c	$k_{\text{mort}}(T) = k_{\text{mort}} \cdot \exp(0.07 \cdot T)$
T dependence for k_{ox}^d	$k_{\text{ox}}(T) = k_{\text{ox}} \cdot 2^{((T - T_{\text{ref}})/10)}$
T dependence for k_{denit}^e	$k_{\text{denit}}(T) = k_{\text{denit}} \cdot 1.07^{(T - T_{\text{ref}})}$
T dependence for k_{nit}^f	$k_{\text{nit}}(T) = k_{\text{nit}} \cdot 1.08^{(T - T_{\text{ref}})}$
$d\text{PHY}/dt = NPP - M$	
$d\text{DSi}/dt = -\text{redsi} \cdot NPP_{\text{DIA}}$	
$d\text{TOC}/dt = -R - D + M$	

Table 3. Continued.

$d\text{NO}_3/dt = -94.4/106 \cdot D - \text{redn} \cdot (1 - f_{\text{NH}_4}) \cdot \text{NPP} + N$
$d\text{NH}_4/dt = \text{redn} \cdot (R - f_{\text{NH}_4} \cdot \text{NPP}) - N$
$d\text{O}_2/dt = -R + f_{\text{NH}_4} \cdot \text{NPP} + 138/106 \cdot (1 - f_{\text{NH}_4}) \cdot \text{NPP} - 2 \cdot N + \text{FO}_2$
$d\text{PO}_4/dt = -\text{redp} \cdot (R + D - \text{NPP})$
$d\text{DIC}/dt = R + D - \text{NPP} - \text{FCO}_2$
$d\text{TAlk}/dt = 15/106 \cdot R + 93.4/106 \cdot D - 2 \cdot N - 15/106 \cdot f_{\text{NH}_4} \cdot \text{NPP} + 17/106 \cdot (1 - f_{\text{NH}_4}) \cdot \text{NPP}$
$d\text{SPM}/dt = D_{\text{SPM}} - E_{\text{SPM}}$

Table 4. Sediment parameters used in C-GEM simulations. * indicates that a linear variation is applied in the tidal river zone. In such cases, reported parameter values correspond to those imposed at the estuarine upper limit. Bold parameters refer to generic assumptions valid in alluvial estuaries, while other parameters are adapted from Volta et al. (2014).

Sediment parameters				
Name	Description [unit]	Value		
		Marine estuary	Mixed estuary	Riverine estuary
g	Acceleration due to gravity [m s^{-2}]	9.81	9.81	9.81
ρ_w	Density of pure water [kg m^{-3}]	1000	1000	1000
w_s	SPM settling velocity [m s^{-1}]	1×10^{-3}	1×10^{-3}	1×10^{-3}
$C_{h,\text{EST}}$	Chézy coefficient in the saline estuary [$\text{m}^{1/2} \text{s}^{-1}$]	60	60	60
$C_{h,\text{TID}}$	Chézy coefficient in the tidal river [$\text{m}^{1/2} \text{s}^{-1}$]	40*	40*	40*
$\tau_{\text{cr,EST}}$	Critical shear stress for erosion and deposition in the saline estuary [N m^{-2}]	0.4	0.4	0.4
$\tau_{\text{cr,TID}}$	Critical shear stress for erosion and deposition in the tidal river [N m^{-2}]	1.0*	1.0*	1.0*
$E_{\text{ero,EST}}$	Erosion coefficient in the saline estuary [$\text{kg m}^{-2} \text{s}^{-1}$]	3.5×10^{-6}	3.5×10^{-6}	3.5×10^{-6}
$E_{\text{ero,TID}}$	Erosion coefficient in the tidal river [$\text{kg m}^{-2} \text{s}^{-1}$]	$6.0 \times 10^{-8*}$	$6.0 \times 10^{-8*}$	$6.0 \times 10^{-8*}$

wind speed and water temperature are extracted from data reported for the coastal temperate zones by the CCMP data set (Atlas et al., 2011) and the World Ocean Atlas global database (<http://www.nodc.noaa.gov/OC5/indprod.html>), respectively. A constant tidal amplitude ($\zeta_0 = 3.5$ m) is applied at the mouth of all estuaries, whereas a different system-specific freshwater discharge is imposed at their upper limits (see Sect. 2.2 and Table 1). Model simulations are forced with two different sets of biogeochemical boundary condition (Table 7). The first set, referred to as the baseline set, is representative of present-day conditions, while the second set represents a scenario for the year 2050. The riverine inputs of organic carbon, nutrients and suspended particulate matter of the baseline set are derived from the global statistical model GlobalNEWS2 (Mayorga et al., 2010). Values represent the average calculated over all watersheds in temperate regions that discharge to the sea through a tidal estuary. For these calculations, we use the estuarine coastal typology of Dürr et al. (2011), which identifies four types of estuaries: small deltas, tidal systems, lagoons and fjords. In this typology, tidal systems (type 2) represent a good approximation of the domain of applicability of C-GEM (Regnier et al., 2013b). NO_3 and NH_4 concentrations are derived

by applying a NH_4/DIN ratio equal to 0.2 to DIN concentrations provided by GlobalNEWS2. The latter is calculated as the median of the NH_4/DIN ratios reported by Meybeck (1982) in more than 40 rivers. Alkalinity is derived from the GLORICH database (Hartmann et al., 2014) and represents the average value for all watersheds in temperate regions. A constant CO_2 concentration typical of temperate rivers worldwide ($\approx 90 \mu\text{M C}$, from 3-year time series in more than 1000 sampling locations; Lauerwald et al., 2015) is then used to calculate dissolved inorganic carbon (DIC) concentration at the upstream limit. Because of the lack of relevant global database and in order to minimize the influence of boundary conditions on estuarine phytoplankton and oxygen profiles, arbitrary low riverine concentrations are imposed for both phytoplanktonic groups (DIA and nDIA), while the saturation concentration is imposed for O_2 . The downstream boundary is located 50 km away from the estuarine mouth in order to minimize its influence on the estuarine biogeochemical dynamics. Here, salinity, organic carbon, nutrient and oxygen concentrations are extracted from data reported for the temperate regions by the World Ocean Atlas global database (<http://www.nodc.noaa.gov/OC5/indprod.html>), while phytoplankton concen-

Table 5. Values of the biogeochemical parameters used in this study. ^a indicates temperature-dependent parameters. ^b and ^c refer to generic parameters estimated from the average and the median of literature values, respectively. Redfield ratios are from Redfield et al. (1963) and Brzezinski (1985). K_{D1} and K_{D2} are from Volta et al. (2014). All rates are defined at 20 °C.

Biogeochemical parameters		
Name	Description [unit]	Value
$P_{\max}^{B\ a,c}$	Maximum specific photosynthetic rate [s^{-1}]	2.58×10^{-5}
α^+	Photosynthetic efficiency [$m^2\ s\ \mu E^{-1}\ s^{-1}$]	4.11×10^{-7}
$k_{\text{maint}}^{a,c}$	Phytoplankton maintenance rate constant [s^{-1}]	4.6×10^{-7}
$k_{\text{mort}}^{a,c}$	Phytoplankton mortality rate constant [s^{-1}]	1.56×10^{-6}
k_{excr}^+	Phytoplankton excretion constant [–]	5.0×10^{-2}
k_{growth}^b	Phytoplankton growth constant [–]	2.9×10^{-1}
K_{D1}	Background light extinction coefficient [m^{-1}]	1.3
K_{D2}	Specific light attenuation of suspended matter [$mg^{-1}\ m^{-1}$]	6.0×10^{-2}
$k_{\text{ox}}^{a,b}$	Aerobic degradation rate constant [$\mu M\ C\ s^{-1}$]	6.08×10^{-4}
$k_{\text{denit}}^{a,c}$	Denitrification rate constant [$\mu M\ C\ s^{-1}$]	5.05×10^{-4}
$k_{\text{nit}}^{a,c}$	Nitrification rate constant [$\mu M\ N\ s^{-1}$]	2.73×10^{-5}
K_{in,O_2}^b	Inhibition term for denitrification [$\mu M\ O_2$]	33.0
K_{DSi}^c	Michaelis–Menten constant for dissolved silica [$\mu M\ Si$]	1.07
$K_{\text{PO}_4}^c$	Michaelis–Menten constant for phosphate [$\mu M\ P$]	0.20
$K_{\text{NH}_4}^b$	Michaelis–Menten constant for ammonium [$\mu M\ N$]	228.9
$K_{\text{NO}_3}^b$	Michaelis–Menten constant for nitrate [$\mu M\ N$]	26.07
K_{TOC}^b	Michaelis–Menten constant for organic carbon [$\mu M\ C$]	186.25
$K_{O_2,ox}^c$	Michaelis–Menten constant for oxygen in aerobic degradation [$\mu M\ O_2$]	31.0
$K_{O_2,nit}^c$	Michaelis–Menten constant for oxygen in nitrification [$\mu M\ O_2$]	51.25
K_N^c	Michaelis–Menten constant for dissolved nitrogen [$\mu M\ N$]	1.13
redsi	Redfield ratio for silica [$mol\ Si\ mol\ C^{-1}$]	15/106
redn	Redfield ratio for nitrogen [$mol\ N\ mol\ C^{-1}$]	16/106
redp	Redfield ratio for phosphorous [$mol\ P\ mol\ C^{-1}$]	1/106

Table 6. Values used for the climate forcings as representative of temperate regions.

Climate forcings	Unit	Value
Water temperature, T	°C	12
Wind speed at the estuarine mouth, WS_0	$m\ s^{-1}$	8
Mean solar radiation, \bar{I}	$\mu E\ m^{-2}\ s^{-1}$	780
Photoperiod, r	h	12

trations are deduced from SeaWIFS data (<http://oceancolor.gsfc.nasa.gov>). TALK and DIC are calculated by assuming a typical seawater pH of 8.2 (Mackenzie et al., 2011) and an average difference between atmospheric and shelf seawater pCO_2 (ΔpCO_2) of 20 μatm for the year 2000 (Cai, 2011) consistent with a CO_2 sink for the coastal ocean under present-day conditions (Bauer et al., 2013; Laruelle et

al., 2014). No database is available to constrain average total organic carbon and suspended particulate matter concentrations at the lower boundary and both concentrations are arbitrarily set to 0. In the case of SPM, the implementation in C-GEM of a sediment transport module allows for enough internal production of SPM to generate realistic profiles along the entire estuarine length. In addition, the low concentration reflects the low values typically observed on the shelf compared to those observed in shallow nearshore areas (e.g., Ruddick et al., 2003). On the other hand, although a variable load of organic carbon can be imported from the adjacent coast into the estuary (e.g., Arndt et al., 2011a) and assuming a TOC concentration of 0 at the lower boundary may thus be an approximation, our choice allows focusing on the fate of organic matter brought the estuary from rivers by minimizing the effect of organic carbon produced and imported from the sea into estuaries. The second biogeochemical boundary condition set represents a future scenario

Table 7. Boundary conditions used for the different scenario simulations.

	Upper boundary		Lower boundary	
	Baseline (year 2000)	Future scenario (year 2050)	Baseline (year 2000)	Future scenario (year 2050)
<i>S</i> [–]	0	0	34	34
DIA [$\mu\text{M C}$]	10	10	1	1
nDIA [$\mu\text{M C}$]	10	10	1	1
NO ₃ [$\mu\text{M N}$]	72	93	5	5
NH ₄ [$\mu\text{M N}$]	18	23	1	1
TOC [$\mu\text{M C}$]	545	514	0	0
DSi [$\mu\text{M Si}$]	87	82	9	9
O ₂ [$\mu\text{M O}_2$]	280	280	280	280
PO ₄ [$\mu\text{M P}$]	3	5	1	1
DIC [$\mu\text{M C}$]	1837	1837	2000	2040
TAlk [$\mu\text{M C}$]	1749	1749	2223	2223
SPM [g L^{-1}]	0.1	0.08	0	0

for the year 2050. The latter assumes a continuous increase of anthropogenic CO₂ emissions (scenario RCP6.0; Moss et al., 2010; IPCC Report, 2013), as well as a rising socio-economic development and a reactive approach to environmental problems (global orchestration scenario; Seitzinger et al., 2010). The global orchestration scenario is used to constrain future riverine inputs of DIN, PO₄, TOC, DSi and SPM by year 2050 (Seitzinger et al., 2010). It predicts an increase of about 29 and 57 % in DIN and PO₄, respectively, essentially induced by increased inputs of sewage, fertilizer and manure, and a decrease in TOC, DSi and SPM of about 6, 5 and 17 %, respectively, owing to the influence of damming. On the other hand, no generic predictions are available for riverine DIC and TAlk concentrations and long time-series analyses indicate diverging trends that are inconclusive (e.g., Jones Jr. et al., 2003; Raymond et al., 2008). As a consequence, no future evolution can be confidently attributed to riverine DIC and TAlk at the moment. Because of the increase in atmospheric CO₂ concentrations, ocean DIC concentrations are expected to increase, while ocean alkalinity will stay constant over the next decades due to the buffering capacity of the ocean (e.g., Andersson et al., 2005; Mackenzie et al., 2011; IPCC Report, 2013). However, the exact magnitude of these variations remains unconstrained and the CO₂ uptake rate by the coastal ocean may double or even triple by year 2050 (Andersson and Mackenzie, 2004; IPCC Report, 2013). Here, future marine DIC concentrations are calculated using MatLab csys.m (Zeebe and Wolf-Gladrow, 2001) by assuming that TAlk does not change in the near future and an average atmospheric $p\text{CO}_2$ of 468 μatm , corresponding to the value predicted by the IPCC RCP6 scenario for the year 2050 (IPCC Report, 2013), while a seawater $p\text{CO}_2$ of 408 μatm is imposed in order to test the influence of an hypothetical future 3-fold increase of the atmospheric and marine water $\Delta p\text{CO}_2$ (i.e., 60 μatm) with respect to the year 2000.

2.4 Biogeochemical indicators

The biogeochemical dynamics of the three representative estuarine systems are investigated and compared by means of four whole-system biogeochemical indicators: the net ecosystem metabolism (NEM), the CO₂ exchange flux with the atmosphere (FCO₂) and the total nitrogen and carbon filtering capacities (FC_{TN} and FC_{TC}, respectively).

2.4.1 Net ecosystem metabolism (NEM)

The NEM is defined as the whole-system difference between net primary production (NPP) and heterotrophic degradation (aerobic degradation + denitrification) (Andersson and Mackenzie, 2004). The NEM is, thus, controlled by the input, export, production and decomposition of terrestrial and in situ-produced organic matter (Odum, 1956) and is typically used to assess the trophic status of an estuary (e.g., Caffrey, 2003; Borges and Abril, 2011). Heterotrophic systems are characterized by the dominance of organic matter degradation over production (NEM < 0), which leads to a net regeneration and export of inorganic carbon and nutrients. In contrast, autotrophic estuaries, dominated by photosynthetic production (NEM > 0), are characterized by a net burial and export of organic matter. As a consequence, the estuarine NEM can be used not only in defining the trophic status of system but also as an indicator of carbon and nutrient sources and sinks in an estuary.

2.4.2 CO₂ exchange flux (FCO₂)

The balance between autotrophic and heterotrophic processes also controls to a large extent the estuarine inorganic carbon dynamics and, thus, the CO₂ exchange across the water–atmosphere interface (FCO₂). In general, FCO₂ depends on the overall effect of biogeochemical processes on dissolved inorganic carbon (DIC) and total alkalinity (TALK). For instance, the aerobic degradation of organic matter generally releases large amounts of DIC, decreases pH and thus promotes CO₂ outgassing, whereas NPP increases water pH and limits CO₂ evasion. Denitrification, on the other hand, increases both DIC and TALK and thus exerts a limited influence on the inorganic carbon budget, while nitrification decreases pH and generally sustains CO₂ outgassing. FCO₂ is, thus, an integrative measure of all biogeochemical processes that exert an influence on the carbonate systems in estuaries (Regnier et al., 2013b).

2.4.3 Nitrogen and carbon filtering capacities (FC_{TN} and FC_{TC})

Total nitrogen and total carbon filtering capacities (FC_{TN} and FC_{TC}, respectively) provide a measure for how much nitrogen or carbon is lost during the estuarine transit. By considering denitrification as the (negative) net process rate affecting estuarine nitrogen, FC_{TN} is calculated as the ratio between denitrification and total riverine nitrogen (TN) flux, defined as the sum of the dissolved inorganic nitrogen and the organic nitrogen bound to living and detrital organic matter (Arndt et al., 2009). Similarly, FC_{TC} is defined as the ratio between carbon loss through the water–atmosphere interface and the total riverine carbon (TC) influx, which accounts for both inorganic and organic carbon (Regnier et al., 2013b). Carbon and nitrogen cycles are typically strongly altered by biogeochemical processes within the estuarine bioreactor and estuarine removal efficiency may thus have relevant implications for the coastal biogeochemistry and for processes producing and releasing greenhouse gases (e.g., N₂O, CO₂) (e.g., Seitzinger, 1988; Soetaert and Hermann, 1995; Voss et al., 2011; Bauer et al., 2013; Regnier et al., 2013a). An analysis of FC_{TN} and FC_{TC} may thus advance the understanding of the role of estuaries in the carbon and nitrogen biogeochemical cycling.

2.5 Sensitivity study

A sensitivity analysis is carried out to assess the response of the biogeochemical indicators (FC_{TN}, FC_{TC}, FCO₂ and NEM) in the three idealized estuaries to variations in aerobic degradation, denitrification and nitrification rate constants (k_{ox} , k_{denit} and k_{nit} , respectively). These parameters are selected because of the heterotrophic character of estuaries (Borges and Abril, 2011; Volta et al., 2014) and the significant effect of nitrification rates on water pH and, thus,

on DIC speciation, water $p\text{CO}_2$ and FCO₂ (Regnier et al., 2013b). The generic rate constants (Table 5) are used as baseline values and are exponentially increased and decreased over 1 order of magnitude. That range of variation corresponds to the range of k_{ox} values reported in the literature and minimum and maximum values may be regarded as representative of refractory and labile organic carbon loads, respectively (see Sect. 3). Similarly, the outermost k_{nit} and k_{denit} values may be considered as representative of different ammonia-oxidizing and nitrate-reducing microbial communities, respectively. For each estuary, 10 parameter combinations are tested. An additional sensitivity test is also performed in which, k_{ox} and k_{denit} vary over 2 orders of magnitude as in the first test (SA1), but k_{nit} remains constant at its baseline value (Table 5). This second sensitivity analysis (SA2) allows assessing the relative importance of the heterotrophic and nitrification reactions on the estuarine biogeochemical indicators in the three idealized estuaries by comparing results from both series of tests. All the parameter values used in SA1 and SA2 are provided in Table A1.

3 Biogeochemical parameter review and analysis

3.1 Literature review

Values for 18 biogeochemical parameters included in the biogeochemical reaction network of the C-GEM modeling platform (Table 3) were compiled by a literature review comprising 49 model applications for tidal estuarine systems in temperate regions (Table 5). The review comprises models of different complexity ranging from 0- to 3-D models, which were developed and applied to investigate different aspect of estuarine biogeochemistry, such as water quality control (e.g., HydroQual Inc., 1987; Lin et al., 2007), bacterial and phytoplankton dynamics (e.g., Robson and Hamilton, 2004; Macedo and Duarte, 2006; Gypens et al., 2013), or estuarine nutrient budgets (e.g., Soetaert and Herman, 1995; Arndt et al., 2009) at different timescales ranging from months to several years. The review covers the following 12 parameters, assumed to be temperature-independent:

- Michaelis–Menten half-saturation constants (K_{DSi} , K_{PO_4} , K_{NH} , K_{NO_3} , K_{TOC} , $K_{O_2,ox}$, $K_{O_2,nit}$, and K_N in μM), which account for the dependency of biogeochemical reaction rates on substrate availability;
- the inhibition constant for denitrification (K_{in,O_2} in $\mu\text{M O}_2$), describing the inhibition of denitrification reaction by oxygen;
- the photosynthetic efficiency (α in $\text{m}^2 \text{s} \mu\text{E}^{-1} \text{s}^{-1}$), which represents the light harvesting efficiency of phytoplankton;
- the phytoplankton excretion (k_{excr}) and growth constants (k_{growth}), accounting for the fraction (in %) of the

gross production lost through exudation processes and the maximum growth of phytoplankton, respectively.

In addition, 6 temperature-dependent parameters (as well as their associated temperature functions) are covered:

- the maximum specific photosynthetic rate (P_{\max}^B in s^{-1}), which corresponds to the light-saturated, carbon uptake rate by primary production;
- the phytoplanktonic maintenance (k_{maint} in s^{-1}) and mortality (k_{mort} in s^{-1}) rate constants, representing the loss of biomass due to maintenance activity and phytoplankton mortality, respectively;
- the rate constants for aerobic degradation (k_{ox} in $\mu\text{M C s}^{-1}$) and denitrification (k_{denit} in $\mu\text{M C s}^{-1}$) describing the reactivity of organic matter towards heterotrophic decay and the nitrification rate constant (k_{nit} in $\mu\text{M N s}^{-1}$), which defines the reactivity of ammonia towards biologically mediated oxidation.

In order to include as many studies as possible, a unit homogenization was performed for the parameters involved in biogeochemical reactions whose mathematical formulations differ from those implemented in C-GEM (Table 3). First-order reaction rate constants of aerobic degradation, denitrification and/or nitrification, expressed in s^{-1} (e.g., Soetaert and Herman, 1995; Robson and Hamilton, 2004; Hofmann et al., 2008), were converted to zero-order constants in $\mu\text{M s}^{-1}$ by multiplying the first-order reaction constant by the typical watershed concentration of the substrate involved in the specific reaction (i.e., TOC for aerobic degradation and denitrification and NH_4 for nitrification). Both TOC and NH_4 concentrations were extracted from the global statistical model GlobalNEWS2 (Mayorga et al., 2010). Watershed-specific NH_4 concentration are estimated on the basis of reported DIN concentrations by assuming a NH_4/DIN ratio of 0.2, representing the median of the NH_4/DIN ratios reported by Meybeck (1982) in more than 40 uncontaminated and polluted rivers worldwide. Similarly, maximum specific photosynthetic rate constants (P_{\max}^B), expressed in $\text{g C g Chl}^{-1} \text{s}^{-1}$ (e.g., Cerco, 2000; Kim and Cerco, 2003; Desmit et al., 2005), are converted to first-order carbon-production-based P_{\max}^B expressed in s^{-1} , by dividing P_{\max}^B in $\text{g C g Chl}^{-1} \text{s}^{-1}$ by the associated carbon-to-chlorophyll ratio in g C g Chl^{-1} . Biogeochemical parameter values reported in the literature are summarized in Fig. 5. The latter shows that, with the exception of P_{\max}^B , for which very large variability (> 35 orders of magnitude) is found, biogeochemical parameter values typically span over a maximum of 5 orders of magnitude. The Michaelis–Menten constant $K_{\text{O}_2, \text{ox}}$ and the inhibition constant for denitrification ($K_{\text{in}, \text{O}_2}$), as well as the phytoplankton parameters α , k_{excr} and k_{growth} , vary over 1 order of magnitude. On the other hand, a variability over 2 orders of magnitude is found for the five Michaelis–Menten terms K_{NH_4} , K_{NO_3} , K_{TOC} , $K_{\text{O}_2, \text{nit}}$, K_{N} , as well as for the phytoplankton

parameter k_{maint} and the rate constant for aerobic degradation (k_{ox}). Finally, the Michaelis–Menten terms K_{DSi} , the mortality rate for phytoplankton, k_{mort} , and the nitrification constant rate (k_{nit}) display a relatively large variability over 3 orders of magnitude, while the Michaelis–Menten parameter K_{PO_4} and the denitrification constant rate (k_{denit}) vary over 4 and 5 orders of magnitude, respectively. The large variability range observed for phytoplankton parameters, such as P_{\max}^B , k_{maint} , k_{mort} and K_{PO_4} , is likely related to the fact that these parameters typically represent different phytoplanktonic species or groups, with varying traits. However, in the reviewed modeling applications, phytoplanktonic parameter values vary not only from a phytoplankton species to another but also within the same group. For example, different k_{maint} values are reported for the same phytoplankton group (i.e., diatoms) in Soetaert et al. (1994), Garnier et al. (1995) and Kim and Cerco (2003). On the other hand, some modeling applications used the same parameter value for different phytoplanktonic groups (e.g., same mortality rate constant for diatoms, flagellates and *Phaeocystis* in Blauw et al., 2009). The literature review also reveals that biogeochemical parameter values do not strongly vary from one estuarine system to another, but different values are also used in modeling studies of the same estuary (e.g., four different k_{ox} values used in modeling applications to the Scheldt estuary by Soetaert and Herman, 1995; Regnier et al., 1997; Regnier and Steefel, 1999; Hofmann et al., 2008; Arndt et al., 2009; Volta et al., 2014).

For the temperature-dependent parameters, corresponding temperature functions are also included in the review. The review reveals that the temperature dependence of the aerobic and the denitrification rate constants (k_{ox} and k_{denit} , respectively) is typically expressed as an exponential increase of the rate constants with temperature (e.g., Regnier et al., 1997; Hofmann et al., 2008; Arndt et al., 2009; Volta et al., 2014). On the other hand, the temperature dependence of autotrophic parameters, such as the nitrification rate constant (k_{nit}), the maximum specific photosynthetic rate (P_{\max}^B), and the phytoplankton maintenance and mortality rate constants (k_{maint} and k_{mort} , respectively) can be implemented as exponential functions, where the parameter value increases with temperature (e.g., Peterson and Festa, 1984; Le Pape and Ménesguen, 1997; Guillaud et al., 2000; Laruelle et al., 2009), or as Gaussian functions, where the value increases until an optimum temperature is reached and then progressively decreases (e.g., Garnier et al., 1995; Kim and Cerco, 2003; Gypens et al., 2013; Zheng et al., 2004).

A summary of the reviewed biogeochemical parameters, as well as their values, the location of the respective modeling studies and the corresponding reference, is provided in Tables B1 and B2. For the temperature-dependent parameters (Table B2), temperature functions are also reported.

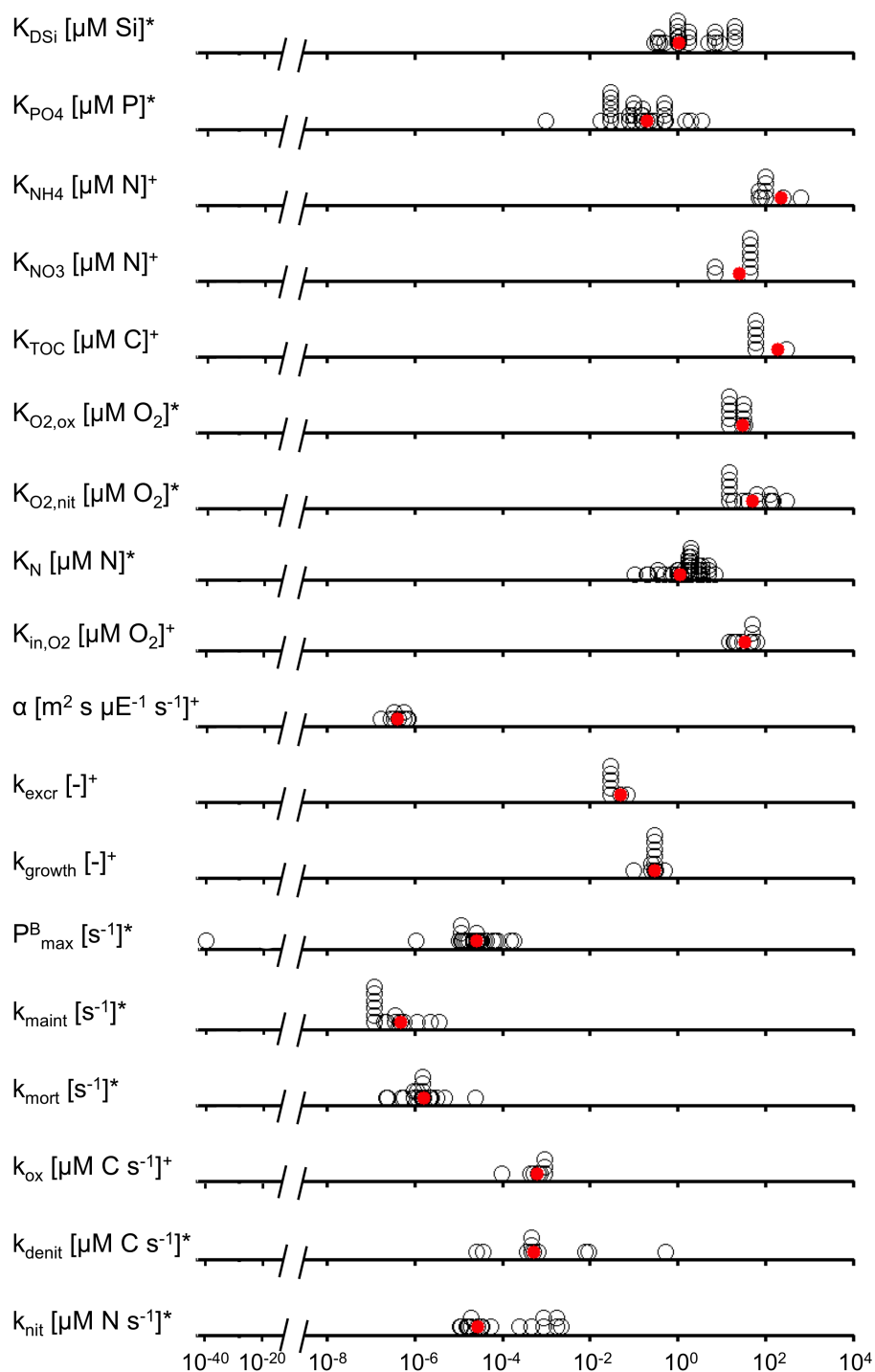


Figure 5. Biogeochemical parameters reported in modeling studies applied to tidal estuaries in temperate regions (black circles) displayed on a logarithmic scale. Red dots represent the values used in this study (see Table 5). * and + indicate when literature parameters showed a skewed or a normal distribution, respectively (refer to Sect. 3.2 for more details). The symbols are stacked when the same parameter value is reported by more than one modeling application. For references and values, see Tables B1 and B2.

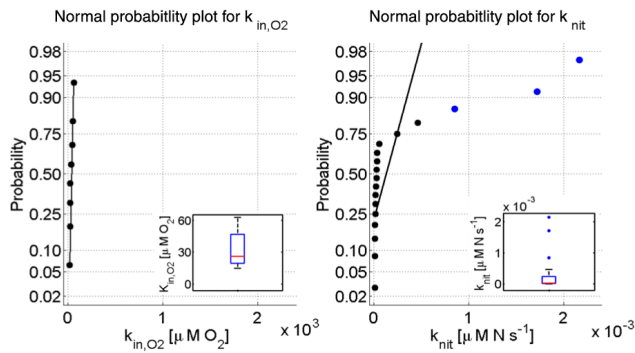


Figure 6. Results from the outlier/distribution analysis for the inhibition term for denitrification (K_{in,O_2} in $\mu\text{M O}_2$; left panel) and for the nitrification rate constant (k_{nit} in $\mu\text{M N s}^{-1}$; right panel). Dots correspond to parameter values from our literature review. The straight black line represents the theoretical normal distribution. In the left panel, K_{in,O_2} reveals a normal distribution, while on the right panel k_{nit} displays a distribution strongly skewed by the presence of outliers (blue dots). Data are plotted on similar scales to facilitate the comparison. In each panel, the inset represents the corresponding whisker plot, where boxes contain literature values included between the 25th and the 75th percentiles; the whiskers extend between the maximum and the minimum, beyond which a value is considered an outlier; and blue dots and red lines represent outlier values and the median of literature values, respectively.

3.2 Parameter analysis

A statistical analysis was performed to determine a generic biogeochemical parameter set representing the mean or the median of the respective published parameter values. Generally, the mean is considered a rigorous estimate of the central tendency of a set of normally distributed numerical scores. However, it is not a well-suited measure for data sets with a skewed distribution since it is largely influenced by outlier values. In this case, a numerical measure able to minimize the outlier influence on the generic trend, such as the median, should be preferred (Mendenhall et al., 2013). Here, the presence of outliers is used to determine whether a biogeochemical parameter may be approximated with the arithmetical mean or the median of a data set. If no outliers are detected, the literature parameter set can be considered normally distributed and thus the generic biogeochemical parameter can be approximated by the mean. Otherwise, when at least one outlier is identified, the distribution of values in the parameter set is assumed to be skewed and the generic biogeochemical parameter is calculated as the median of the literature values (Fig. 6). Parameter values are classified as outliers if they are larger than $q_3 + w \cdot (q_3 - q_1)$ or smaller than $q_1 - w \cdot (q_3 - q_1)$, where q_1 and q_3 are the 25th and 75th percentiles, respectively, while w is the maximum whisker length. The latter is set equal to 1.5, which corresponds to approximately 99 % coverage if the data are normally distributed and represents a rational compromise

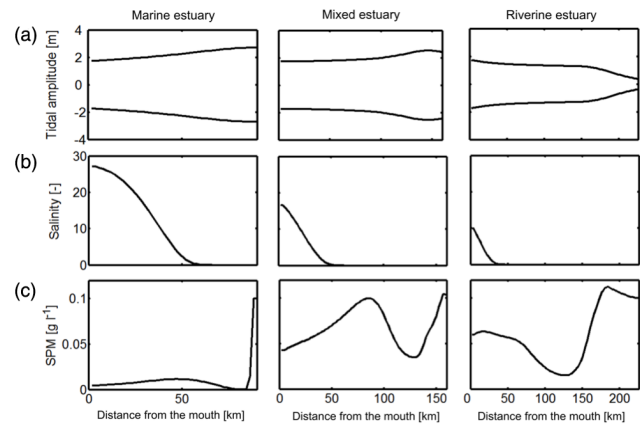


Figure 7. Longitudinal distributions of tidal amplitude (a), computed as difference between simulated maximum/minimum and average water depths, salinity (b) and SPM (c), modeled in the three representative estuaries using parameters listed in Tables 1 and 4 and baseline boundary conditions reported in Table 7.

between a rigorous parameter value selection, which aims to identify a generic tendency of the literature parameter distributions without being influenced by values too high or too low compared to the rest of the sample, and the conservation of a statistically relevant number of parameter values.

For the sake of generalization, although in some modeling applications phytoplankton parameters were associated with specific groups, no distinctions between different phytoplankton species and/or groups were made during the analysis and any numerical value was assigned the same weight in the parameter estimation. Therefore, the generic set of phytoplankton parameters derived here should represent a generic estuarine phytoplankton group. Moreover, when a modeling study reported different aerobic degradation and denitrification rate constants (k_{ox} and k_{denit} , respectively) for differently reactive organic matter pools (e.g., Soetaert and Herman, 1995; Schroeder, 1997; Hofmann et al., 2008), the value considered in the parameter analysis corresponds to the average value of the two constants reported. Therefore, the generic values for k_{ox} and k_{denit} may be regarded as representative of organic matter decomposition through high-energy-yielding metabolic pathways.

A generic set of temperature functions, associated with temperature-dependent biogeochemical parameters, is derived by analyzing the T functions reported by the reviewed modeling applications. For phytoplankton temperature-dependent parameters, generic temperature functions were preferentially chosen over group-specific temperature formulations. For the phytoplankton maintenance rate constants (k_{maint}), all temperature functions reported in the literature referred to specific phytoplanktonic groups. In this case, the function associated with the largest number of different phytoplankton groups was considered the most generic and, thus, retained. On the other hand, although all tempera-

ture functions reported in the literature for aerobic degradation and denitrification rate constants are exponential, they nevertheless show different trends depending on the initial values and exponential factors applied. In this case, the formulation showing the average trend is selected as generic function (refer to Fig. B1). Finally, for the temperature function associated with the rate constant of nitrification (k_{nit}), the most frequently used function is chosen (refer to Table B2 for more details). For the generic temperature functions of biogeochemical parameters as implemented in C-GEM, refer to Table 3.

4 Results and discussion

4.1 Hydrodynamics and salt transport

In an estuarine system, the interplay between tidal and fluvial influence results in important longitudinal variations in tidal amplitude and salinity (Fig. 7a and b). The comparison of the simulated longitudinal tidal amplitude and the salinity profiles for the three representative estuaries (Table 1) reflects the strong mutual dependency between estuarine geometry and hydrodynamic characteristics.

The distortion of the tidal wave in upstream direction (Fig. 7a) is mainly controlled by the balance between energy gain due to channel convergence and energy loss through friction. In the marine estuary, the strong convergence of the estuarine banks (short convergence length) compensates for the energy loss through friction and the tidal amplitude increases landward to 5.5 m at the upper estuarine boundary. In the mixed estuary, on the other hand, the weak amplification of the tidal amplitude indicates that the energy gain through convergence is almost balanced by the energy lost through friction. Upstream, tidal amplitude increases more rapidly to reach a maximum of about 5 m where convergence and friction effect are both of low magnitude. Beyond this point, close to the inland limit, the relative importance of the friction increases, owing to a relatively higher fluvial energy, and triggers a slight dampening of the tidal amplitude. In the riverine estuary, the weak channel convergence (long convergence length) combined with the dominant fluvial influence leads to a dampening of the tidal amplitude, in particular in the upper reach where frictional energy loss reaches a maximum. In summary, the marine and the mixed estuaries are typically characterized by a net energy gain through convergence and thus by a tidal amplitude amplification along their longitudinal gradients, whereas the large fluvial influence always induces a net reduction of estuarine energy by bottom friction and a consequent tidal damping in the riverine system.

In alluvial estuaries, the salinity intrusion is controlled by the balance between upstream dispersion and downstream advective transport and, thus, by the system's geometric and hydrodynamic properties (Savenije, 2005, 2012). Simulated

salinity profiles for the three idealized systems (Fig. 7b) reflect this dependency. Despite identical lower boundary conditions ($S = 34$ at 50 km beyond the estuarine mouth; see Sect. 2.3.5), the shape of the simulated salinity profile and, in particular, the salinity gradient close to the estuarine mouth, as well as the salt intrusion length, reveal the characteristic differences generally observed across the different estuarine types (Savenije, 1992, 2005, 2012). These differences can be largely attributed to the relative significance of the tidal versus the fluvial influence in each system. The marine estuary is characterized by a dominant tidal influence and, thus, a small salinity gradient close to the mouth ($\Delta S = 7$), a concave salinity profile and a long salinity intrusion length of almost the 75 % of the total estuarine length (EL). On the other hand, in the mixed estuary, tidal and fluvial influences are of roughly equal importance and the salinity gradient close to the mouth is thus larger than in the marine estuary ($\Delta S = 17$). Moreover, the larger fluvial influence, results in a recession shape profile and a shorter salinity intrusion length of 40 % of the EL. Similarly, the riverine estuary displays a recession-shape salinity profile. However, the salinity gradient at the estuarine mouth is much larger ($\Delta S = 24$) and the salinity intrusion shorter (20 % of the EL) than in the mixed system due to the large riverine discharge and the smaller tidal exchange.

4.2 Solid transport

In alluvial estuaries, the main features of the longitudinal distribution of suspended particulate matter (SPM) can be linked to the mechanical energy provided by the tides and the riverine discharge (Jay et al., 1990; Dalrymple et al., 1992). The longitudinal SPM profiles simulated in the marine and the mixed estuary reveal similar SPM trends (Fig. 7c). In both cases, SPM concentrations increase in the lower estuary due to the progressive compression of the incoming flood into a smaller cross-sectional area and to a consequent increase in the flood-tidal current speed and reach locally high values where the total energy (fluvial + tidal) is maximal, while, further upstream, SPM concentrations decrease to a minimum at the so-called balance point, where fluvial and tidal energy contributions are of similar but low magnitude. In the upper reaches, SPM concentrations are largely controlled by the riverine influence. The progressive decrease in fluvial energy from the upper estuarine limit to the sea induces a reduction of erosion and a consequent increase in deposition rates. As a result, decreasing SPM from the upper limit to the energy balance point is simulated. On the other hand, the riverine estuary reveals two turbidity maxima separated by a zone of low SPM concentrations, corresponding to the energetic balance point (Fig. 7c). As for the marine and the mixed cases, the progressive increase in SPM from the downstream limit upwards is essentially related to the progressive compression of the marine inflow into a progressively smaller volume. Nonetheless, in the upper reaches, maximum SPM concen-

trations are likely induced by the high river discharges promoting net erosion, as well as by the strong volumetric reduction associated with the large tidal wave dampening (Fig. 7a). A quantitative comparison of the SPM concentrations simulated in the three representative estuaries (Fig. 7c) reveals that the marine system shows very low SPM levels. The latter are likely related to the strong funnel character of this system that, bearing relatively steeper and larger volumetric variations along the estuarine gradient (Fig. 3), entails a larger dilution effect on SPM concentrations. Overall, modeled SPM distributions agree well with the conceptual, mechanical energy patterns described by Dalrymple et al. (1992), who identified two high-energy zones separated by a low-energy area (the balance point) in tidal estuaries. Moreover, they indicate that the extent of these zones along the three idealized estuaries, as well as their sediment loads, can be strongly affected by different hydro-geometrical characteristics.

4.3 Biogeochemistry

4.3.1 Biogeochemical dynamics – baseline simulations

Figure 8 shows the longitudinal distribution of ammonium (NH_4), nitrate (NO_3), phosphate (PO_4), dissolved silica (DSi), oxygen (O_2), total organic carbon (TOC), diatoms (DIA), non-diatom phytoplankton (nDIA), dissolved inorganic carbon (DIC), total alkalinity (TALK), pH and water $p\text{CO}_2$ in the three idealized estuaries simulated with the set of baseline boundary conditions (Table 7).

Simulated concentration and biogeochemical rate profiles reveal several characteristic features that are common across the three estuaries. In addition, although a direct quantitative comparisons with observations is difficult, the simulated concentration and rate profiles qualitatively agree with observed chemical distributions from different temperate tidal systems, such as, for instance, the Chesapeake Bay (e.g., Horrigan et al., 1990) and the Delaware (e.g., Sharp et al., 2009), the Scheldt (e.g., Baeyens et al., 1998), the Thames and the Gironde (e.g., Frankignoulle et al., 1998), the Severn (e.g., Jonas and Millward, 2010) and the Tweed (Howland et al., 2000) estuaries. TOC and nutrient (NH_4 , NO_3 , PO_4 and DSi) concentrations show an overall decrease in downstream direction (Fig. 8a) due to dilution and high reaction rates in the upper reaches of the estuarine systems (Fig. 9). However, the estuarine profiles of NH_4 and PO_4 reveal a mid-estuary maximum (Fig. 8a), which results from the slow degradation of TOC in this area (Fig. 8a). Although slightly positive net primary production rates are simulated in the upper estuaries, average annual conditions (e.g., temperature, photoperiod and solar irradiation) prevent the occurrence of phytoplanktonic blooms and phytoplankton concentrations (DIA and nDIA, Fig. 8a) progressively decrease downstream due to dilution and phytoplankton mortality effects. The lower reaches are consistently characterized by high O_2 , DIC and TALK concentrations and a high pH, which decrease in up-

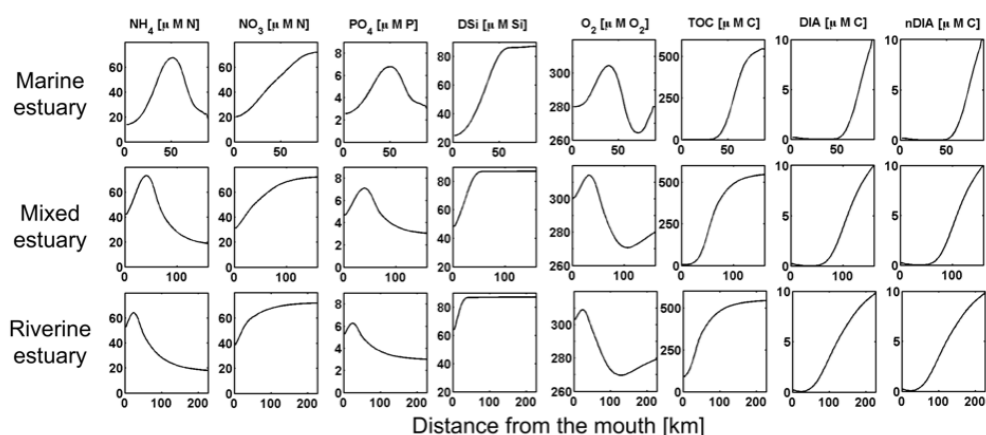
Table 8. Biogeochemical indicators calculated for the three idealized estuaries by using the baseline and the future boundary conditions (columns a and b, respectively). NEM and FCO_2 are in kmol C day^{-1} , while FC_{TN} and FC_{TC} are expressed as percentage of the total riverine input. FCO_2 is negative when towards the atmosphere. Integrated rates for NEM's constitutive reactions are also provided (R : aerobic degradation in kmol C day^{-1} ; D : denitrification in kmol C day^{-1} ; NPP: net primary production in kmol C day^{-1}). Relative variations in biogeochemical indicators (and NEM's constitutive reactions) compared to their baseline values, are also reported in column b (values inside brackets). MAR, MIX and RIV correspond to the marine, the mixed and the riverine estuary, respectively.

Biogeochemical indicator [unit]	Estuarine type	Scenario simulation	
		(a) Baseline (year 2000)	(b) Future (Year 2050)
NEM [kmol C day^{-1}]	MAR		−916
		R	859
		D	79
		NPP	22
	MIX		−8161
		R	7664
		D	492
		NPP	−5
	RIV		−21 476
		R	20 199
		D	1299
		NPP	21
FCO_2 [kmol C day^{-1}]	MAR		−2018
	MIX		−10 940
	RIV		−25 612
FC_{TN} [%]	MAR		22
	MIX		18
	RIV		15
FC_{TC} [%]	MAR		40
	MIX		30
	RIV		22

stream direction. Aerobic degradation is by far the dominant pathway of organic carbon degradation in all estuaries (Fig. 9a) and, together with the O_2 transfer across the air–water interface, it is the dominant control on the O_2 longitudinal distribution (Fig. 9b). TALK profiles are essentially determined by total heterotrophic degradation (aerobic degradation + denitrification) and nitrification (Fig. 9d), while DIC concentrations largely depend on a dynamic balance between production via aerobic degradation and loss through CO_2 outgassing (Fig. 9e). These two processes are also the main drivers of the pH changes along the longitudinal axis of all estuaries (Fig. 9f). In the upper reaches, maximum $p\text{CO}_2$ concentrations (Fig. 8b) correspond to the areas where minimum pH values are simulated.

Although the three idealized estuarine types reveal similar biogeochemical dynamics, they also show distinct features. In particular, the increasing significance of freshwa-

(a) Organic carbon dynamics



(b) Inorganic carbon dynamics

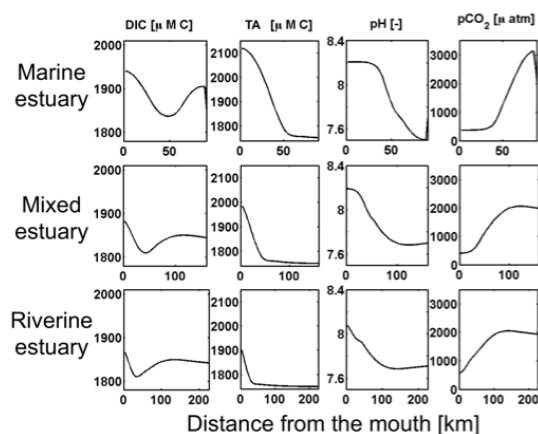


Figure 8. Longitudinal distributions of chemical species involved in organic (a) and inorganic carbon (b) dynamics in the three representative estuaries. Simulations are forced with parameters reported in Tables 1, 4 and 5 and with the baseline biogeochemical boundary conditions summarized in Table 7.

ter discharge from the marine to the riverine estuary results in a stronger residual transport in downstream direction, which systematically pushes the biogeochemical fronts towards the estuarine mouth. Large quantitative differences between the three idealized estuaries are also evident when comparing the values of their integrated biogeochemical indicators (Table 8, column a). Although results show that all estuaries are net heterotrophic ($\text{NEM} < 0$) and act as net sources for atmospheric CO_2 ($\text{FCO}_2 < 0$), the system-scale NEM and FCO_2 increase from the marine (-916 and $-2018 \text{ kmol C day}^{-1}$, respectively) to the mixed (-8161 and $-10940 \text{ kmol C day}^{-1}$) and to the riverine system (-21476 and $-25612 \text{ kmol C day}^{-1}$) due to the strong correlation between these indicators and the riverine influx (Regnier et al., 2013b; refer to Tables 1 and 7). Yet, the nitrogen and carbon filtering capacities (FC_{TN} and FC_{TC} , respectively) decrease from the marine to the riverine type (Table 8, column a), reflecting the progressively shorter transit times

of the water masses as the discharge increases (e.g., Nixon et al., 1996; Arndt et al., 2009, 2011a; Regnier et al., 2013b). The simulated integrative measures of NEM and FCO_2 for the three idealized estuaries, ranging between -2 and $-39 \text{ mol C m}^{-2} \text{ yr}^{-1}$ and -4 and $-47 \text{ mol C m}^{-2} \text{ yr}^{-1}$, respectively, fall within the range of values observed in tidal estuaries in temperate regions (-63 to $+25.1$ and -76 to $+6 \text{ mol C m}^{-2} \text{ yr}^{-1}$ for NEM and FCO_2 , respectively; refer to Borges and Abril, 2011, and Laruelle et al., 2013, for a complete list of values). Furthermore, N filtering capacities of the three systems (15–22 %) are comparable to typical values reported in the literature for temperate tidal estuaries, such as the Seine (< 7 –40 %; Garnier et al., 2001), the Scheldt (13–78 %; Arndt et al., 2009) and the James (24–40 %; Bukaveckas and Isenberg, 2013) estuary, while their C-removal efficiencies (22–40 %) are comparable to the range calculated in Regnier et al. (2013b) for three idealized, western European tidal estuaries (25–31 %).

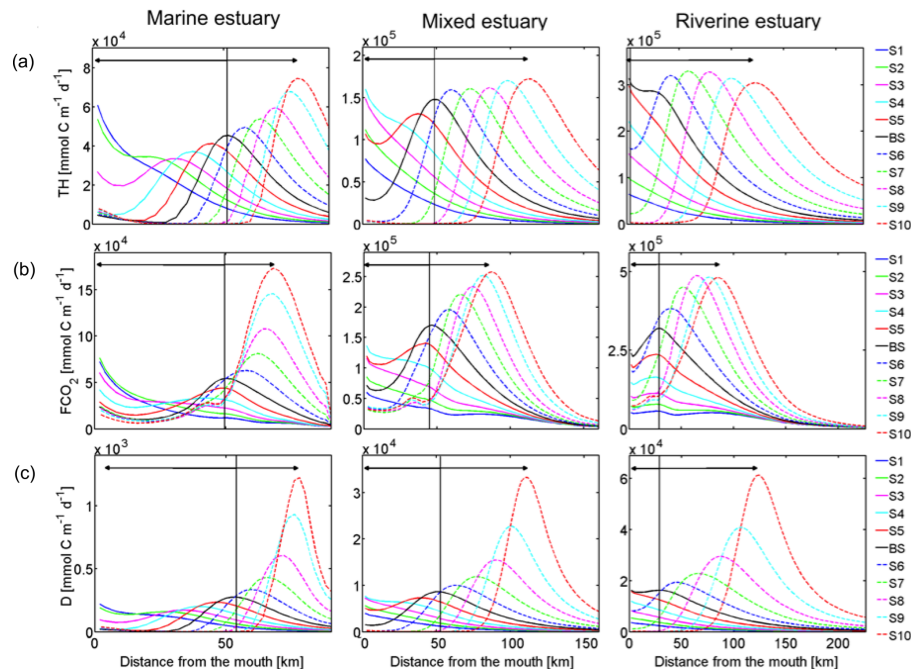


Figure 11. Longitudinal profiles of (a) total heterotrophic degradation (TH, in $\text{mmol C m}^{-1} \text{ day}^{-1}$), (b) CO₂ outgassing (FCO₂, in $\text{mmol C m}^{-1} \text{ day}^{-1}$) and (c) denitrification (D , in $\text{mmol C m}^{-1} \text{ day}^{-1}$) rates in the three idealized estuaries for each of the simulations of the first sensitivity analysis (SA1; see Table A1). S1 to S10 refer to different simulations, each corresponding to a specific parameter combination while BS indicates baseline parameter values (Table 5). Black vertical lines indicate the position of the maximal rates simulated by using the BS biogeochemical parameter sets, while arrows displays the longitudinal shift of the biogeochemical fronts by varying reaction rate constants.

to the total organic carbon input flux of each estuary as a relative measure of the amount of organic carbon that is processed within the estuary (FC_{org} in Fig. 10b). In the marine estuary, FC_{org} is high and weakly sensitive to variations in rate constants. On the other hand, in the mixed and the riverine estuary, FC_{org} is high and fairly constant when parameter values are larger than BS values, but rapidly decreases when reducing k_{ox} , k_{denit} and k_{nit} below their BS values. Above the BS threshold, a rapid degradation of organic matter results in a significant consumption of the organic carbon flux (about 90 % of the riverine flux) irrespective of the estuarine type. These results emphasize the delicate balance between reaction timescales and residence time in determining filtering capacities. In general, increasing the values of the rate constants above BS values shifts the heterotrophic degradation zone further upstream in all estuaries (Fig. 11a), where residence times are, due to smaller volumes, shorter. However, although the shape and the peak value of the total heterotrophic longitudinal profile vary, the integrated degradation rates and thus the FC_{org} are similar across estuaries (Fig. 10a and b). Therefore, results reveal that differences in geometrical characteristics do not exert a strong influence on organic carbon dynamics. On the other hand, a reduction of kinetic rate constants below BS values triggers a downstream shift of the heterotrophic zone (Fig. 11a). Here, larger

volumes and thus longer residence times may partly compensate for the low reaction rates. This is particularly true for the marine estuary, where the long residence time strongly compensates for the reduced rate constants and translates in high and fairly constant FC_{org}, while the continuous decrease in FC_{org} values simulated in the mixed and the riverine estuary suggests that the increase in residence time is not sufficient to compensate for low reaction rates.

Figure 10c and d summarizes the FCO₂ and the FC_{TC} simulated in the three idealized estuaries for the set of rate constants SA1. Since the C filtering capacity depends on the estuarine efficiency in scavenging carbon through CO₂ degassing, FC_{TC}'s and FCO₂'s sensitivity results are discussed together. As for the NEM, the strong correlation between FCO₂ and system-specific riverine carbon inputs limits the quantitative comparison of the FCO₂ variability across the three systems. However, a qualitative analysis reveals that CO₂ outgassing (FCO₂ < 0) increases with increasing parameter values in all systems. As a consequence, enhanced C-removal efficiencies, which increase from the riverine to the marine estuary, are also simulated. Closer inspection of the different responses suggests that decreasing k_{ox} , k_{denit} and k_{nit} below BS values only induces small FC_{TC} variations in the marine estuary, whereas a larger sensitivity is simulated in the mixed and the riverine estuaries. Such behavior

is very similar to that of the NEM and further confirms that system-specific differences in residence time play an important role in controlling the estuarine biogeochemical functioning when reaction rates are low and biogeochemical reaction zones are pushed further downstream (Fig. 11b). On the other hand, increasing k_{ox} , k_{denit} and k_{nit} above BS values results in a larger sensitivity in the marine estuary, where FC_{TC} can reach values up to 90 %, while the mixed and the riverine systems only reveal a weak sensitivity and fairly constant FC_{TC} values (about 40 %). These differences reflect the direct dependence of FCO_2 on gas exchange and thus the estuarine surface area. As shown in Fig. 11b, increasing rate constants above BS values induces an upstream shift of the zone where maximum CO_2 degassing occurs. Here, smaller surface areas may, however, partly limit the gas exchange. This is particularly true for the mixed and the riverine systems, where long convergence length and thus comparably smaller surface areas limit the potential positive effect of higher reaction rate constants on CO_2 outgassing. In contrast, the large increase in FC_{TC} simulated in the marine estuary by increasing k_{ox} , k_{denit} and k_{nit} above BS values suggests that its strong funnel-shaped character, entailing relatively larger surface, always allows for enhanced C-removal efficiencies even if the FCO_2 front is located in the upper zone.

The FC_{TN} sensitivities in the three idealized estuaries to changes in parameter combinations are presented in Fig. 10e. The close similarity between the results obtained for FC_{TN} and FC_{TC} suggests that N removal is also controlled by residence time when the rate constants decrease below BS values and the denitrification zone is pushed further seawards (Fig. 11c). However, unlike FC_{TC} , the progressive FC_{TN} increase simulated in the three idealized estuaries by increasing the rate constants indicates that denitrification and, thus, FC_{TN} could theoretically be enhanced by a further increase in rate constants in all systems.

The comparison of the results from the two sensitivity tests (SA1 and SA2 in Fig. 10) shows that nitrification rate constants exert small effects on all biogeochemical indicators in the three idealized estuaries. Slightly larger variations are simulated for FCO_2 (and consequently for FC_{TC}), as well as for FC_{TN} , by varying the k_{nit} value and reflect the biogeochemical coupling between nitrification and inorganic carbon dynamics (higher nitrification promotes CO_2 outgassing) and between nitrification and denitrification (higher nitrification promotes higher denitrification), respectively. On the other hand, although varying k_{nit} may also potentially influence estuarine NEM (and thus FC_{org}) through the nitrification–denitrification and nitrification–primary production couplings as implemented in the C-GEM biogeochemical module (refer to Table 3), virtually no effects are simulated, confirming that aerobic degradation is by far the dominant process in controlling the organic carbon dynamics in the three idealized estuaries.

4.4 Future scenarios

The potential effects of future environmental changes on the biogeochemical functioning of estuaries are assessed by comparing the biogeochemical indicators (NEM, FCO_2 , FC_{TN} and FC_{TC}) simulated under baseline conditions (year 2000) with those simulated using a future scenario representing the year 2050 (Table 7). Results and integrated rates for the reactions influencing the NEM are summarized in Table 8. Compared to the biogeochemical boundary conditions of the baseline run, the future scenario using the global orchestration projections (Seitzinger et al., 2010) predicts an increase in PO_4 and dissolved inorganic nitrogen ($\text{DIN} = \text{NH}_4 + \text{NO}_3$) loads from rivers (+57 and +29 %, respectively), as well as a decrease in TOC, DSI and SPM (−6, −1 and −17 %, respectively). Simulation results indicate that, in 2050, NEM will still be dominated by heterotrophic degradation and all estuaries will remain largely net heterotrophic (Table 8), although a slight improvement of the estuarine trophic status (less negative NEM values compared to baseline conditions) is simulated. These results essentially reflect the effect of increasing nutrient and decreasing TOC and SPM concentrations on primary production and heterotrophic degradation reactions. In particular, the larger nutrient and light availability, promoting higher NPP rates, and the smaller organic carbon input from rivers, sustaining lower degradation rates, translate into a less negative NEM in all three idealized systems in the future (Table 8). In quantitative terms, the magnitude of NEM variations in the three estuaries is always smaller than 6 %, because the influence of NPP on the overall carbon balance, as well as the predicted drop in organic carbon inputs from rivers, is marginal.

Table 8 also reveals that the CO_2 outgassing flux from the three idealized estuarine systems will decrease in the future. While such trends may appear to contradict a simulated increase in water $p\text{CO}_2$ (data not shown) and decrease in pH (Fig. 12a), the higher atmospheric $p\text{CO}_2$ expected in 2050 (468 μatm) actually leads to a net decrease in the $p\text{CO}_2$ gradient at the air–water interface and to an acidification of the estuarine water masses. As a consequence, the three estuaries will become less important CO_2 sources for the atmosphere in 2050 because the atmospheric CO_2 increase will largely offset the estuarine CO_2 increase (Fig. 12b, Table 8). Furthermore, Table 8 indicates that the mixed and the riverine estuaries reveal low sensitivities to increased atmospheric CO_2 concentrations (−8 and −4 % in CO_2 evasion for the mixed and the riverine cases, respectively), while the marine estuary shows a larger reduction in CO_2 outgassing (−20 %). Although all estuaries remain net CO_2 sources for atmosphere in 2050 when the exchange rate is integrated over the entire estuarine volume, a reversal trend is simulated in the downstream zone of the marine estuary, which will become a net sink for atmospheric CO_2 (Fig. 12b). On the other hand, the mixed and the riverine systems will remain atmospheric CO_2 sources all along their longitudinal profiles. These re-

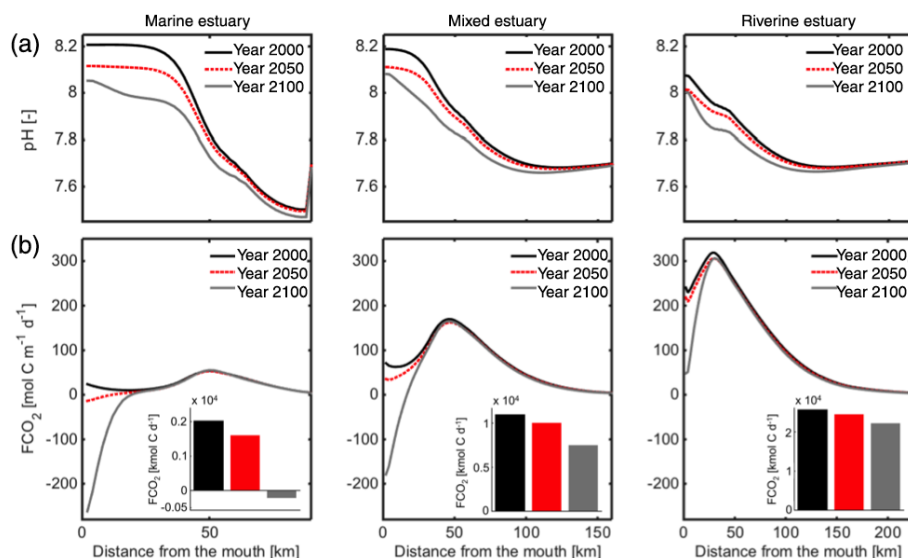


Figure 12. Longitudinal distributions of pH (a) and depth- as well as width-integrated FCO₂ (b) simulated using a biogeochemical scenario for years 2000 and 2050 in the three idealized estuaries. Note that results from simulations carried out until year 2100 are also reported. The bar graphs in the lower panels represent the volume-integrated FCO₂ for the three simulated years (data are plotted on a different y axis scale). Positive FCO₂ values represent CO₂ emissions, while negative values correspond to CO₂ flux from the atmosphere towards the water.

sults essentially reflect the different influences of the adjacent coastal zone on the estuarine biogeochemistry in the three systems. If simulations are carried out until year 2100, assuming a $p\text{CO}_2$ gradient as high as 234 μatm at the marine boundary and an atmospheric $p\text{CO}_2$ of 660 μatm (Moss et al., 2010), the downstream zone of the marine estuary could become strongly undersaturated with respect to the atmospheric equilibrium and largely compensate for CO₂ outgassing in the upper reaches (Fig. 12b). For instance, volume-integrated CO₂ exchange rate over the entire domain indicates that the marine estuary might become a sink for atmospheric CO₂ in 2100. Furthermore, a sink zone could develop in the mixed estuary in 2100, while the riverine system will remain a net source (Fig. 12b).

By definition, FC_{TC} depends on CO₂ outgassing and on the TC riverine input flux. Therefore, the overall decrease in CO₂ emissions simulated in the future in the three idealized systems translates into consistent reductions in FC_{TC} (Table 8). Finally, simulation results also reveal that the efficiency of the three estuaries in removing nitrogen will decrease in the future (FC_{TN} in Table 8), because the projected increase in riverine nitrogen loads (+29 %) is comparatively larger than the enhanced nitrogen removal through denitrification simulated in each idealized estuary (D in Table 8). The outcomes of our scenarios are in overall agreement with the future increase in carbon and nitrogen export to the coastal ocean predicted at global scale (e.g., Kroeze and Seitzinger, 1998; Bauer et al., 2013). Although these projections can only be regarded as a first-order estimate for future trends because of the great deal of uncertainty in predicting future conditions, our findings highlight that, by the end of the century,

changes in carbon and nutrient loads from the catchments may lead to a significantly smaller impact on the overall estuarine C balance than the atmospheric CO₂ increase. Furthermore, the latter may be such that estuaries under strong marine influence could experience a shift from being net CO₂ sources to net CO₂ sink, in a manner similar to that already advocated for the coastal ocean (e.g., Mackenzie et al., 2004; Bauer et al., 2013; Regnier et al., 2013a).

5 Conclusions and outlook

A generic modeling approach was used to quantitatively explore the biogeochemical dynamics across three idealized alluvial estuaries (marine, mixed and riverine) and to relate their behavior to their main hydro-geometrical characteristics. To this end, a comprehensive literature review of biogeochemical parameter values (e.g., rate and half-saturation constants) used in estuarine model applications was performed. This allowed deriving a generic set of parameter values for our simulations including reasonable ranges to perform sensitivity tests. This large literature survey, to our knowledge the first of its kind, highlighted that modeling studies are largely biased towards temperate latitudes. Out of a total of 51 modeling applications, 49 are from temperate regions and two are from the tropics (see map provided in the Supplement). Results from our simulations performed for typical temperate conditions (30–60° in either hemisphere) are in line with recent literature syntheses (Borges and Abril, 2011; Laruelle et al., 2013) showing that the vast majority of estuaries are net heterotrophic and act as net sources for at-




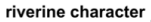
Freshwater discharge, Q			
Width convergence length, b			
	<div><div>marine character</div><div></div><div>riverine character</div></div>		
Sensitivity to k_{ox}, k_{denit} and k_{ox} :			
Trophic status (NEM in kmol C d^{-1})	-900 to -1000	-2500 to -8100	-2800 to -25200
CO_2 degassing (FCO_2 in kmol C d^{-1})	1500 to 4200	3700 to 15200	7000 to 39500
Nitrogen filtering capacity (FC_{TN} in %)	16 to 46	5 to 40	2 to 39
Carbon filtering capacity (FC_{TC} in %)	31 to 85	10 to 41	6 to 34
Future behaviors (year 2050) :			
Metabolic status (ΔNEM)	-5 %	- 6 %	-4 %
CO_2 degassing (ΔFCO_2)	-20 %	-8 %	-4 %
Nitrogen filtering capacity ($\Delta\text{FC}_{\text{TN}}$)	-9 %	-9 %	-8 %
Carbon filtering capacity ($\Delta\text{FC}_{\text{TC}}$)	-19 %	-7 %	-5 %

Figure 13. Main results of the sensitivity analysis and scenario simulations summarized as functions of the key hydro-geometrical parameters: freshwater discharge (Q in $\text{m}^3 \text{s}^{-1}$) and width convergence length (b in m). Results of the sensitivity analysis report ranges corresponding to the maximum and minimum values obtained for any parameter combination of the sensitivity analysis SA1. Results of the scenario simulations are expressed in percentages of relative change between years 2000 and 2050.

mospheric CO_2 . The average C filtering capacities for baseline conditions are 40, 30 and 22 % for the marine, mixed and riverine estuary, respectively. Extrapolating these filtration rates to the carbon loads of all temperate tidal estuaries worldwide, as defined in Dürr et al. (2011), results in a regional outgassing flux between 0.01 and 0.02 PgC yr^{-1} , assuming that the total amount of carbon delivered by rivers to these systems is 0.06 PgC yr^{-1} (calculated from Hartmann et al., 2009, and Mayorga et al., 2010). Moreover, a global CO_2 outgassing comprised between 0.04 and 0.07 PgC yr^{-1} can be calculated by extending these calculations to all tidal estuaries worldwide and assuming that the global amount of carbon delivered by rivers is then 0.17 PgC yr^{-1} (calculated from Hartmann et al., 2009, and Mayorga et al., 2010). Since this estimate ignores that tropical and polar tidal estuaries may process riverine carbon differently than temperate systems, it only represents a first-order quantification of the CO_2 outgassing flux from tidal estuaries worldwide. Nonetheless, it is broadly in line with the recent global estimate calculated by Laruelle et al. (2013) (0.06 PgC yr^{-1}). In addition, results for baseline conditions indicate that the three idealized estuaries can retain between 15 and 22 % of the total nitrogen input from the land. On the other hand, sensitivity analysis performed by varying the rate constants for aerobic degradation, denitrification and nitrification over the range of values reported in the literature significantly widens these ranges (Fig. 13). Although the bulk of published N and C retention rates are generally based on local studies (e.g., Soetaert and Herman, 1995; Regnier and Steefel, 1999; Arndt et al., 2009; Billen et al., 2009), while literature syntheses are limited (Nixon et al., 1996; Laruelle, 2009; Regnier et al., 2013b), our estimates confirm the importance of considering the estuarine filter in global and regional C and N budgets.

Overall, our simulations using three idealized estuaries allow identifying the main influence of a marine or riverine character of a system on its biogeochemical functioning (Fig. 13). For instance, simulation results suggest that marine estuaries with short width convergence length (banks that strongly converge in the landward direction) could be efficient filters for nitrogen but relatively limited sources for atmospheric CO_2 . In contrast, mixed and riverine estuaries, owing to their relatively large CO_2 outgassing, could contribute disproportionately to the global estuarine CO_2 budget. The presented approach could thus ultimately enhance our ability to transfer knowledge from well-known estuaries to poorly constrained systems and to predict their biogeochemical functioning even when available data are scarce. Helpful insights are also provided by the sensitivity analysis, which reveals that, for the parameter ranges tested, the uncertainty in aerobic degradation and denitrification rates may translate into large specific-system responses. Finally, prospective simulations for the year 2050 indicate that, while the riverine and mixed estuaries will remain heterotrophic and only marginally affected by river load changes and increase in atmospheric $p\text{CO}_2$, the marine estuary is likely to become a significant CO_2 sink in its downstream section. Such a change in behavior might offset the current balance between the CO_2 emitted by estuaries and that taken up by continental shelf seas (Andersson et al., 2005; Laruelle et al., 2010, 2013, 2014; Cai, 2011; Bauer et al., 2013; Regnier et al., 2013a).

Although this study provides advances on the qualitative and quantitative understanding of the estuarine biogeochemistry in tidal estuaries, our approach also relies on simplifications and abstractions. As a consequence, even if simulation results may be considered as representative of the main tidal, alluvial estuarine classes, they only represent a limited num-

ber of estuarine cases that may not cover the extremely wide spectrum of hydro-geometrical and biogeochemical properties typically observed in estuaries. For instance, our sensitivity results may not be valid in autotrophic estuaries, where primary production rather than heterotrophic processes controls the estuarine biogeochemistry. In addition, the use of the generic modeling platform C-GEM, whose reaction network does not include an early diagenetic model at this stage, hampers the generalization of simulation results to estuaries that are typically subject to intense biogeochemical processing in sediments. For instance, the lack of a representation of denitrification in sediment might result in overestimations of the N export to the coastal ocean. As a consequence, the implementation of an early diagenetic model for carbon, nutrients and O₂ will be the next logical step to further improve our modeling strategy.

In the future, our generic approach could be applied to perform ensemble runs in order to reduce the predictive uncertainty by covering a wider range of hydro-geometrical characteristics and the uncertainty associated with biogeochemical parameters and conditions, as well as climatological regimes. This design will ultimately provide a better understanding of the estuarine dynamics. Moreover, we believe that a generic approach such as ours can be combined with continuously growing high-resolution environmental databases and, coupled to Earth system models, could be used to derive robust regional and/or global biogeochemical mass budgets by explicitly incorporating the estuarine filter into the estimates.

Appendix A: Sensitivity tests

Table A1. List of the parameter values for aerobic degradation (k_{ox}), denitrification (k_{denit}) and nitrification (k_{nit}) rate constants used for the two sensitivity analyses (SA1 and SA2). S1 to S10 refer to different simulations, each corresponding to a specific parameter combination, while BS indicates baseline parameter values (see Sect. 2.3.4, Table 5).

	Sensitivity analysis 1 (SA1)			Sensitivity analysis 2 (SA2)		
	k_{ox} [$\mu\text{M C day}^{-1}$]	k_{denit} [$\mu\text{M C day}^{-1}$]	k_{nit} [$\mu\text{M N day}^{-1}$]	k_{ox} [$\mu\text{M C day}^{-1}$]	k_{denit} [$\mu\text{M C day}^{-1}$]	k_{nit} [$\mu\text{M N day}^{-1}$]
S1	6.08×10^{-5}	5.05×10^{-5}	2.73×10^{-6}	6.08×10^{-5}	5.05×10^{-5}	2.73×10^{-5}
S2	9.64×10^{-5}	8.00×10^{-5}	4.33×10^{-6}	9.64×10^{-5}	8.00×10^{-5}	2.73×10^{-5}
S3	1.53×10^{-4}	1.27×10^{-4}	6.86×10^{-6}	1.53×10^{-4}	1.27×10^{-4}	2.73×10^{-5}
S4	2.42×10^{-4}	2.01×10^{-4}	1.09×10^{-5}	2.42×10^{-4}	2.01×10^{-4}	2.73×10^{-5}
S5	3.84×10^{-4}	3.19×10^{-4}	1.72×10^{-5}	3.84×10^{-4}	3.19×10^{-4}	2.73×10^{-5}
BS	6.08×10^{-4}	5.05×10^{-4}	2.73×10^{-5}	6.08×10^{-4}	5.05×10^{-4}	2.73×10^{-5}
S6	9.64×10^{-4}	8.00×10^{-4}	4.33×10^{-5}	9.64×10^{-4}	8.00×10^{-4}	2.73×10^{-5}
S7	1.53×10^{-3}	1.27×10^{-3}	6.86×10^{-5}	1.53×10^{-3}	1.27×10^{-3}	2.73×10^{-5}
S8	2.42×10^{-3}	2.01×10^{-3}	1.09×10^{-4}	2.42×10^{-3}	2.01×10^{-3}	2.73×10^{-5}
S9	3.84×10^{-3}	3.19×10^{-3}	1.72×10^{-4}	3.84×10^{-3}	3.19×10^{-3}	2.73×10^{-5}
S10	6.08×10^{-3}	5.05×10^{-3}	2.73×10^{-4}	6.08×10^{-3}	5.05×10^{-3}	2.73×10^{-5}

Appendix B: Parameter review

Table B1. Values of temperature-independent biogeochemical parameters reported from the literature for which a parameter analysis was performed. Outlier values are indicated in *italic*.

Temperature-independent biogeochemical parameters [unit]			
Value	Continent	Location	References
α , photosynthetic efficiency [$\text{m}^2 \text{s} \mu\text{E}^{-1} \text{s}^{-1}$]			
1.67×10^{-7}	Europe	Scheldt estuary	Gypens et al. (2013)
2.76×10^{-7}	Europe	Tagus estuary	Macedo and Duarte (2006)
2.77×10^{-7}	Europe	Scheldt estuary	Gypens et al. (2013)
2.90×10^{-7}	Europe	Scheldt estuary	Vanderborght et al. (2007)
3.33×10^{-7}	Europe	Seine estuary; Scheldt estuary	Garnier et al. (1995), Gypens et al. (2013)
4.17×10^{-7}	Europe	Hypothetical river-coastal zone	Billen and Garnier (1997)
5.80×10^{-7}	Europe	Scheldt estuary	Arndt et al. (2007, 2009), Volta et al. (2014)
6.67×10^{-7}	Europe	Scheldt estuary	Gypens et al. (2013)
6.94×10^{-7}	Europe	Scheldt estuary	Gypens et al. (2013)
k_{excr} , phytoplankton excretion constant [–]			
3.0×10^{-2}	Europe	Scheldt estuary	Desmit et al. (2005), Arndt et al. (2007, 2009), Vanderborght et al. (2007), Volta et al. (2014)
5.0×10^{-2}	S. America	Río de la Plata estuary	Huret et al. (2005)
7.0×10^{-2}	Europe	Ria de Aveiro	Trancoso et al. (2005)
k_{growth} , phytoplankton growth constant [–]			
1.0×10^{-1}	Europe	Tagus estuary	Mateus et al. (2012)
2.5×10^{-1}	Europe; N. America	Chesapeake Bay; Tagus estuary	Cerco and Noel (2004), Mateus et al. (2012)
3.0×10^{-1}	Europe	Carlingford Lough; Scheldt estuary	Ferreira et al. (1998), Desmit et al. (2005), Arndt et al. (2007, 2009), Vanderborght et al. (2007), Volta et al. (2014)
3.2×10^{-1}	Europe	Scheldt estuary	Vanderborght et al. (2002)
5.0×10^{-1}	Europe	Scheldt estuary	Gypens et al. (2013)
$K_{\text{in}, \text{O}_2}$, inhibition term for denitrification [$\mu\text{M O}_2$]			
15.0	Europe	Scheldt estuary	Regnier et al. (1997)
19.0	Australia	Swan estuary	Robson and Hamilton (2004)
20.0	Europe	Scheldt estuary	Vanderborght et al. (2002)
22.0	Europe	Scheldt estuary	Hofmann et al. (2008)
30.0	Europe	Scheldt estuary	Regnier and Steefel (1999)
44.0	Europe	Scheldt estuary	Soetaert and Herman (1995)
50.0	Europe	Scheldt estuary	Vanderborght et al. (2007), Arndt et al. (2009), Volta et al. (2014)
63.0	Europe	Urdaibai estuary	Garcia et al. (2010)

Table B1. Continued.

K_{DSi} , Michaelis–Menten constant for dissolved silica [$\mu\text{M Si}$]			
0.30	Europe	Tagus estuary	Mateus et al. (2012)
0.36	N. America	Chester River and Eastern Bay; Chesapeake Bay	Kim and Cerco (2003), Cerco and Noel (2004)
0.40	Europe	Scheldt estuary	Gypens et al. (2013)
0.50	Europe	Hypothetical river-coastal zone	Billen and Garnier (1997)
1.00	Europe	Bay of Seine; Bay of Brest	Le Pape and Ménesguen (1997), Le Pape et al. (1999), Guillaud et al. (2000), Cugier et al. (2005), Laruelle et al. (2009)
1.07	N. America	Chester River and Eastern Bay; Chesapeake Bay	Kim and Cerco (2003), Cerco and Noel (2004)
1.79	Asia; N. America; Europe	Kwangyang Bay; Chesapeake Bay; Scheldt estuary	Cerco and Cole (1994), Soetaert et al. (1994), Park et al. (2005)
5.00	Australia	Swan estuary	Griffin et al. (2001)
7.00	Europe	Hypothetical river-coastal zone; Scheldt estuary	Billen and Garnier (1997), Arndt et al. (2011a), Gypens et al. (2013)
8.93	Europe	Seine estuary	Garnier et al. (1995)
20.00	Europe	Scheldt estuary	Arndt et al. (2007, 2009), Vanderborght et al. (2007), Volta et al. (2014)
K_{PO_4} , Michaelis–Menten constant for phosphate [$\mu\text{M P}$]			
0.001	Europe	Scheldt estuary	Gypens et al. (2013)
0.02	Asia	Kwangyang Bay	Lee et al. (2005)
0.03	N. America; Europe	Potomac estuary; James estuary; Chesapeake Bay; Satilla estuary; Urdaibai estuary; Scheldt estuary	Thomann and Fitzpatrick (1982) (from Lung and Paerl, 1988), Lung (1986) (via Lung and Paerl, 1988), Cerco and Cole (1994), Zheng et al. (2004), Garcia et al. (2010), Gypens et al. (2013)
0.05	N. America	Chesapeake Bay	HydroQual Inc. (1987) (via Lung and Paerl, 1988)
0.08	N. America	Chester River and Eastern Bay; Chesapeake Bay	Kim and Cerco (2003), Cerco and Noel (2004)
0.10	N. America; Europe	Derwent estuary; Scheldt estuary; Bay of Seine	Guillaud et al. (2000), Cugier et al. (2005), Wild-Allen et al. (2009), Gypens et al. (2013)
0.15	Europe	Bay of Seine	Guillaud et al. (2000), Cugier et al. (2005)
0.16	N. America; Australia; Europe	Neuse estuary; Swan estuary; Curonian lagoon	Lung and Paerl (1988), Griffin et al. (2001) Zemlys et al. (2008)
0.20	Europe	Hypothetical river-coastal zone	Billen and Garnier (1997)
0.23	Europe	Seine estuary	Garnier et al. (1995)
0.32	Europe	Venice lagoon	Solidoro et al. (2005)
0.50	Europe	Hypothetical river-coastal zone; Scheldt estuary	Billen and Garnier (1997), Arndt et al. (2011a), Gypens et al. (2013), Volta et al. (2014)
0.52	Australia	Swan estuary	Griffin et al. (2001)
1.49	Europe	Seine estuary	Garnier et al. (1995)
1.50	Europe	Hypothetical river-coastal zone	Billen and Garnier (1997)
2.00	Europe	Scheldt estuary	Gypens et al. (2013)
3.58	Europe	Venice lagoon	Canu et al. (2003)
K_{NO_3} , Michaelis–Menten constant for nitrate [$\mu\text{M N}$]			
7.14	N. America	Chesapeake Bay; Chester River and Eastern Bay	Cerco and Cole (1994), Kim and Cerco (2003)
45.00	Europe	Scheldt estuary	Regnier and Steefel (1999), Arndt et al. (2007, 2009), Vanderborght et al. (2007), Hofmann et al. (2008), Volta et al. (2014)

Table B1. Continued.

K_{NH_4} , Michaelis–Menten constant for ammonium [μMN]			
71.43	N. America	Chesapeake Bay; Chester River and Eastern Bay	Cerco and Cole (1994), Kim and Cerco (2003)
80.00	Europe	Scheldt estuary	Gypens et al. (2013)
100.00	Europe	Scheldt estuary	Arndt et al. (2007, 2009), Vanderborght et al. (2007), Volta et al. (2014)
250.00	Europe	Scheldt estuary	Regnier and Steefel (1999)
643.00	Europe	Scheldt estuary	Soetaert and Herman (1995)
K_{TOC} , Michaelis–Menten constant for organic carbon [μMC]			
60.00	Europe	Scheldt estuary	Regnier and Steefel (1999), Arndt et al. (2007, 2009), Vanderborght et al. (2007), Volta et al. (2014)
312.50	Europe	Scheldt estuary	Soetaert and Herman (1995)
$K_{\text{O}_2, \text{ox}}$, Michaelis–Menten constant for oxygen in aerobic degradation [$\mu\text{M O}_2$]			
15.00	Europe	Scheldt estuary	Regnier and Steefel (1999), Arndt et al. (2007, 2009), Vanderborght et al. (2007), Volta et al. (2014)
30.00	Europe	Scheldt estuary	Hofmann et al. (2008)
31.00	Australia	Derwent estuary	Wild-Allen et al. (2009)
31.25	N. America; Australia	Chesapeake Bay; Chester River and Eastern Bay; Swan estuary	Cerco and Cole (1994), Kim and Cerco (2003), Robson and Hamilton (2004)
34.00	Europe	Scheldt estuary	Soetaert and Herman (1995)
$K_{\text{O}_2, \text{nit}}$, Michaelis–Menten constant for oxygen in nitrification [$\mu\text{M O}_2$]			
15.00	Europe	Scheldt estuary	Regnier and Steefel (1999), Arndt et al. (2007, 2009), Vanderborght et al. (2007), Volta et al. (2014)
19.00	Europe	Scheldt estuary	Gypens et al. (2013)
30.00	Europe	Scheldt estuary	Hofmann et al. (2008)
31.00	Australia	Derwent estuary	Wild-Allen et al. (2009)
40.00	N. America	Satilla estuary	Zheng et al. (2004)
62.50	N. America	Chesapeake Bay; Chester River and Eastern Bay	Cerco and Cole (1994), Kim and Cerco (2003)
125.00	Europe	Venice lagoon; Urdaibai estuary	Canu et al. (2003), Garcia et al. (2010)
142.86	Europe	Curonian lagoon	Zemlys et al. (2008)
156.00	Europe	Scheldt estuary	Soetaert and Herman (1995)
312.50	Australia	Swan estuary	Robson and Hamilton (2004)

Table B1. Continued.

K_N , Michaelis–Menten constant for dissolved nitrogen [$\mu\text{M N}$]			
0.10	Asia	Kwangyang Bay	Lee et al. (2005)
0.20	Australia	Derwent estuary	Wild-Allen et al. (2009)
0.21	Europe	Seine estuary	Garnier et al. (1995)
0.36	N. America; Europe	James estuary; Seine estuary	Lung (1986) (via Lung and Paerl, 1988), Garnier et al. (1995)
0.50	Europe; S. America	Hypothetical river-coastal zone; Scheldt estuary; Río de la Plata estuary	Billen and Garnier (1997), Huret et al. (2005), Gypens et al. (2013)
0.71	N. America	Chesapeake Bay	Cerco and Cole (1994)
0.80	Europe	Scheldt estuary	Gypens et al. (2013)
1.00	Europe	Ria de Aveiro; Scheldt estuary	Trancoso et al. (2005), Gypens et al. (2013)
1.07	N. America	Chesapeake Bay; Neuse estuary	HydroQual Inc. (1987) (via Lung and Paerl, 1988), Lung and Paerl (1988)
1.19	Europe	Carlingford Lough	Ferreira et al. (1998)
1.43	Australia; N. America	Chester River and Eastern Bay	Griffin et al. (2001), Kim and Cerco (2003)
1.79	N. America; Europe	Potomac estuary; Neuse estuary; Chester River and Eastern Bay; Chesapeake Bay; Urbai bai estuary	Thomann and Fitzpatrick (1982) (via Lung and Paerl, 1988), Lung and Paerl (1988), Kim and Cerco (2003), Cerco and Noel (2004), Garcia et al. (2010)
2.00	N. America; Europe	Satilla estuary; Scheldt estuary; Bay of Seine; Bay of Brest	Le Pape and Ménesguen (1997), Le Pape et al. (1999), Guillaud et al. (2000), Zheng et al. (2004), Cugier et al. (2005), Laruelle et al. (2009), Gypens et al. (2013)
3.00	Europe	Bay of Seine; Bay of Brest	Le Pape et al. (1999), Guillaud et al. (2000), Cugier et al. (2005)
3.50	Europe	Bay of Seine	Le Pape and Ménesguen (1997)
3.57	Europe	Venice lagoon; Curonian lagoon	Canu et al. (2003), Solidoro et al. (2005), Zemlys et al. (2008)
5.00	Europe	Scheldt estuary; hypothetical river-coastal zone	Billen and Garnier (1997), Arndt et al. (2011a), Volta et al. (2014)
7.14	Europe	Scheldt estuary	Soetaert et al. (1994)

Table B2. Values of temperature-dependent biogeochemical parameters reported from the literature for which a parameter analysis was performed. T corresponds to the temperature in °C. T_{abs} is the absolute temperature. All parameter values are normalized at 20 °C. $P_{\text{max,L}}^{\text{B}}$, $k_{\text{main,L}}$, $k_{\text{mort,L}}$, $k_{\text{ox,L}}$, $k_{\text{denit,L}}$ and $k_{\text{nit,L}}$ represent the parameter values reported in the corresponding literature source (refer to references). * indicates that the parameter value is calculated from the mean of values reported for reactive and refractory organic carbon. ** indicates that the parameter value refers to the mean of values associated with different salinities. Outlier values are indicated in italic.

Temperature-dependent biogeochemical parameters [unit]				
Value at 20 °C	T function	Continent	Location	References
$P_{\text{max}}^{\text{B}}$, maximum specific photosynthetic rate [s^{-1}]				
7.16×10^{-41}	$P_{\text{max}}^{\text{B}}(T) = P_{\text{max,L}}^{\text{B}} \cdot \exp\left(-\frac{(T - 5.5)^2}{1.6^2}\right)$	Europe	Scheldt estuary	Gypens et al. (2013)
1.07×10^{-6}	$P_{\text{max}}^{\text{B}}(T) = P_{\text{max,L}}^{\text{B}} \cdot \exp\left(-\frac{(T - 12)^2}{5^2}\right)$	Europe	Hypothetical river-coastal zone	Billen and Garnier (1997)
1.02×10^{-5}	$P_{\text{max}}^{\text{B}}(T) = P_{\text{max,L}}^{\text{B}} \cdot \exp\left(-\frac{(T - 37)^2}{17^2}\right)$	Europe	Seine estuary	Garnier et al. (1995)
1.17×10^{-5}	$P_{\text{max}}^{\text{B}}(T) = P_{\text{max,L}}^{\text{B}} \cdot \exp(0.07 \cdot T)$	Europe	Bay of Seine	Peterson and Festa (1984), Le Pape et al. (1999), Guillaud et al. (2000)
1.23×10^{-5}	$P_{\text{max}}^{\text{B}}(T) = P_{\text{max,L}}^{\text{B}} \cdot \exp\left(-\frac{(T - 25)^2}{5^2}\right)$	Europe	Scheldt estuary	Arndt et al. (2011a)
1.38×10^{-5}	$P_{\text{max}}^{\text{B}}(T) = P_{\text{max,L}}^{\text{B}} \cdot \exp\left(-\frac{(T - 21)^2}{13^2}\right)$	Europe	Seine estuary	Garnier et al. (1995)
1.49×10^{-5}	$P_{\text{max}}^{\text{B}}(T) = P_{\text{max,L}}^{\text{B}} \cdot \exp\left(-\frac{(T - 13)^2}{21^2}\right)$	Europe	Hypothetical river-coastal zone	Billen and Garnier (1997)
1.66×10^{-5}	$P_{\text{max}}^{\text{B}}(T) = P_{\text{max,L}}^{\text{B}} \cdot \exp(0.07 \cdot T)$	Europe	Bay of Seine	Cugier et al. (2005)
2.11×10^{-5}	$P_{\text{max}}^{\text{B}}(T) = P_{\text{max,L}}^{\text{B}} \cdot \exp(0.07 \cdot T)$	Europe	Bay of Brest	Le Pape et al. (1999)
2.31×10^{-5}	$P_{\text{max}}^{\text{B}}(T) = P_{\text{max,L}}^{\text{B}} \cdot 1.067^{(T-20)}$	Europe	Urdaibai estuary	Garcia et al. (2010)
2.34×10^{-5}	$P_{\text{max}}^{\text{B}}(T) = P_{\text{max,L}}^{\text{B}} \cdot \exp\left(-\frac{(T - 15)^2}{12^2}\right)$	Europe	Scheldt estuary	Gypens et al. (2013)
2.35×10^{-5}	$P_{\text{max}}^{\text{B}}(T) = P_{\text{max,L}}^{\text{B}} \cdot \exp(0.07 \cdot T)$	Europe	Bay of Seine	Cugier et al. (2005)
2.58×10^{-5}	$P_{\text{max}}^{\text{B}}(T) = P_{\text{max,L}}^{\text{B}} \cdot \exp(0.07 \cdot T)$	Europe	Bay of Seine	Le Pape and Ménesguen (1997), Guillaud et al. (2000)
2.76×10^{-5}	$P_{\text{max}}^{\text{B}}(T) = P_{\text{max,L}}^{\text{B}} \cdot \exp\left(-\frac{(T - 37)^2}{12^2}\right)$	Europe	Scheldt estuary	Gypens et al. (2013)
2.80×10^{-5}	$P_{\text{max}}^{\text{B}}(T) = P_{\text{max,L}}^{\text{B}} \cdot \exp\left(-\frac{(T - 15)^2}{12^2}\right)$	Europe	Scheldt estuary	Gypens et al. (2013)
3.31×10^{-5}	$P_{\text{max}}^{\text{B}}(T) = P_{\text{max,L}}^{\text{B}} \cdot \exp\left(-\frac{(T - 17)^2}{37^2}\right)$	Europe	Hypothetical river-coastal zone	Billen and Garnier (1997)
3.75×10^{-5}	$P_{\text{max}}^{\text{B}}(T) = P_{\text{max,L}}^{\text{B}} \cdot \exp\left(-\left(0.0018 \cdot (T - 16)^2\right)\right)$	N. America	Chester River and Eastern Bay	Kim and Cerco (2003)
3.86×10^{-5}	$P_{\text{max}}^{\text{B}}(T) = P_{\text{max,L}}^{\text{B}} \cdot \exp\left(-\left(0.0025 \cdot (T - 20)^2\right)\right)$	N. America	Chesapeake Bay	Cerco (2000)
4.38×10^{-5}	$P_{\text{max}}^{\text{B}}(T) = P_{\text{max,L}}^{\text{B}} \cdot \exp\left(-\left(0.0025 \cdot (T - 25)^2\right)\right)$	N. America	Chesapeake Bay	Cerco (2000)
6.10×10^{-5}	$P_{\text{max}}^{\text{B}}(T) = P_{\text{max,L}}^{\text{B}} \cdot \exp\left(-\left(0.0035 \cdot (T - 29)^2\right)\right)$	N. America	Chester River and Eastern Bay	Kim and Cerco (2003)
6.90×10^{-5}	$P_{\text{max}}^{\text{B}}(T) = P_{\text{max,L}}^{\text{B}} \cdot \exp\left(-\frac{(T - 21)^2}{13^2}\right)$	Europe	Scheldt estuary	Gypens et al. (2013)

Table B2. Continued.

6.95×10^{-5}	$P_{\max}^B(T) = P_{\max,L}^B \cdot \exp\left(-\frac{(T-37)^2}{17^2}\right)$	Europe	Scheldt estuary	Gypens et al. (2013)
7.00×10^{-5}	$P_{\max}^B(T) = P_{\max,L}^B \cdot \exp\left(-\frac{(T-15)^2}{12^2}\right)$	Europe	Scheldt estuary	Gypens et al. (2013)
7.55×10^{-5}	$P_{\max}^B(T) = P_{\max,L}^B \cdot \exp\left(-\frac{(0.004 \cdot (T-29)^2)}{1}\right)$	N. America	Chester River and Eastern Bay	Kim and Cerco (2003)
1.58×10^{-4}	$P_{\max}^B(T) = 1.47 \times 10^{-5} \cdot ((1/50) + \exp(0.33 + 0.102 \cdot T))$	Europe	Scheldt estuary	Volta et al. (2014)
1.82×10^{-4}	$P_{\max}^B(T) = P_{\max,L}^B \cdot \exp((T-10)/(\ln(2.075/10)))$	Europe	Scheldt estuary	Soetaert et al. (1994)
k_{maint} , phytoplankton maintenance rate constant [s^{-1}]				
1.16×10^{-7}	$k_{\text{maint}}(T) = k_{\text{maint,L}} \cdot \exp(0.0322 \cdot (T-20));$ $k_{\text{maint}}(T) = k_{\text{maint,L}} \cdot \exp(0.069 \cdot (T-20))$	N. America	Chesapeake Bay; Chester River and Eastern Bay; Pamlico Sound; Cape Fear estuary	Cerco and Cole (1994) Cerco (2000) Kim and Cerco (2003) Cerco and Noel (2004) Lin et al. (2007, 2008)
2.06×10^{-7}	$k_{\text{maint}}(T) = k_{\text{maint,L}} \cdot \exp\left(-\frac{(T-37)^2}{17^2}\right)$	Europe	Seine estuary	Garnier et al. (1995)
2.30×10^{-7}	$k_{\text{maint}}(T) = k_{\text{maint,L}} \cdot \exp(0.0322 \cdot (T-20))$	N. America	Chesapeake Bay	Cerco and Noel (2004)
3.50×10^{-7}	$k_{\text{maint}}(T) = k_{\text{maint,L}} \cdot \exp(0.0322 \cdot (T-20))$	N. America; Asia	Chester River and Eastern Bay; Kwangyang Bay	Kim and Cerco (2003), Park et al. (2005)
4.63×10^{-7}	$k_{\text{maint}}(T) = k_{\text{maint,L}} \cdot \exp(0.069 \cdot (T-20))$	N. America	Chesapeake Bay	Cerco and Cole (1994)
5.57×10^{-7}	$k_{\text{maint}}(T) = k_{\text{maint,L}} \cdot \exp\left(-\frac{(T-21)^2}{13^2}\right)$	Europe	Seine estuary	Garnier et al. (1995)
1.16×10^{-6}	$k_{\text{maint}}(T) = k_{\text{maint,L}} \cdot \exp((T-10) \cdot \ln(2)/10)$	Europe	Scheldt estuary	Soetaert et al. (1994)
2.30×10^{-6}	$k_{\text{maint}}(T) = k_{\text{maint,L}} \cdot \exp(0.0322 \cdot (T-20))$	N. America	Chesapeake Bay	Cerco (2000)
3.50×10^{-6}	$k_{\text{maint}}(T) = k_{\text{maint,L}} \cdot \exp(0.0322 \cdot (T-20))$	N. America	Chester River and Eastern Bay	Kim and Cerco (2003)

Table B2. Continued.

k_{mort} , phytoplankton mortality rate constant [s^{-1}]				
2.30×10^{-7}	–	N. America	Potomac estuary	Thomann and Fitzpatrick (1982) (via Lung and Paerl, 1988)
2.35×10^{-7}	$k_{\text{mort}}(T) = k_{\text{mort,L}} \cdot \exp(0.07 \cdot T)$	Europe	Thau lagoon	Chapelle et al. (2000)
5.15×10^{-7}	$k_{\text{mort}}(T) = k_{\text{mort,L}} \cdot \exp\left(-\left((T - 37)^2\right)/17^2\right)$	Europe	Seine estuary	Garnier et al. (1995)
5.80×10^{-7}	–	N. America	Neuse estuary	Lung and Paerl (1988)
9.33×10^{-7}	$k_{\text{mort}}(T) = k_{\text{mort,L}} \cdot \exp(0.07 \cdot T)$	Europe	Bay of Brest	Le Pape et al. (1999) Laruelle et al. (2009)
1.16×10^{-6}	–	N. America	James estuary; Chesapeake Bay	Lung (1986) (via Lung and Paerl, 1988), HydroQual Inc. (1987) (via Lung and Paerl, 1988)
1.41×10^{-6}	$k_{\text{mort}}(T) = k_{\text{mort,L}} \cdot \exp(0.07 \cdot T)$	Europe	Bay of Seine	Guillaud et al. (2000)
1.47×10^{-6}	$k_{\text{mort}}(T) = k_{\text{mort,L}} \cdot \exp((T - 10) \cdot \ln(2.075)/10)$	Europe	Scheldt estuary	Arndt et al. (2007, 2009), Arndt and Regnier (2007), Volta et al. (2014)
1.64×10^{-6}	$k_{\text{mort}}(T) = k_{\text{mort,L}} \cdot \exp(0.07 \cdot T)$	Europe	Bay of Seine	Guillaud et al. (2000)
2.09×10^{-6}	$k_{\text{mort}}(T) = k_{\text{mort,L}} \cdot \exp\left(-\left((T - 21)^2\right)/13^2\right)$	Europe	Seine estuary	Garnier et al. (1995)
2.26×10^{-6}	$k_{\text{mort}}(T) = k_{\text{mort,L}} \cdot 2^{((T-15)/10)}$	Australia	Derwent estuary	Wild-Allen et al. (2009)
2.30×10^{-6}	–	N. America	Chesapeake Bay	HydroQual Inc. (1987) (via Lung and Paerl, 1988)
2.35×10^{-6}	$k_{\text{mort}}(T) = k_{\text{mort,L}} \cdot \exp(0.07 \cdot T)$	Europe	Bay of Brest	Le Pape et al. (1999)
3.25×10^{-6}	$k_{\text{mort}}(T) = k_{\text{mort,L}} \cdot 1.072^T$	Europe	Venice lagoon; Veerse Meer	Blauw et al. (2009)
4.73×10^{-6}	$k_{\text{mort}}(T) = k_{\text{mort,L}} \cdot 1.085^T$	Europe	Venice lagoon; Veerse Meer	Blauw et al. (2009)
2.35×10^{-5}	$k_{\text{mort}}(T) = k_{\text{mort,L}} \cdot \exp(0.07 \cdot T)$	Europe	Bay of Vilaine	Chapelle et al. (1994)
k_{ox} , aerobic degradation rate constant [$\mu\text{M C s}^{-1}$]				
9.75×10^{-5}	–	N. America	Chester River and Eastern Bay	Kim and Cerco (2003)
$4.43 \times 10^{-4*}$	$k_{\text{ox}}(T) = k_{\text{ox,L}} \cdot \exp((T - 10) \cdot \ln(1.65)/10)$	Europe	Scheldt estuary	Soetaert and Herman (1995)
$5.06 \times 10^{-4*}$	$k_{\text{ox}}(T) = k_{\text{ox,L}} \cdot 2^{((T-15)/10)}$	Europe	Scheldt estuary	Hofmann et al. (2008)
6.66×10^{-4}	–	N. America	Chester River and Eastern Bay	Kim and Cerco (2003)
7.35×10^{-4}	$k_{\text{ox}}(T) = k_{\text{ox,L}} \cdot 1.08^{(T-20)}$	Australia	Swan estuary	Robson and Hamilton (2004)
7.38×10^{-4}	$k_{\text{ox}}(T) = k_{\text{ox,L}} \cdot 10^{((T_{\text{abs}}-278.15)/22.6)}$	Europe	Scheldt estuary	Regnier et al. (1997)
$7.50 \times 10^{-4*}$	$k_{\text{ox}}(T) = k_{\text{ox,L}} \cdot 1.047^{(T-20)}$	Europe	Elbe estuary	Schroeder (1997)
9.26×10^{-4}	$k_{\text{ox}}(T) = k_{\text{ox,L}} \cdot 2.75^{((T_{\text{abs}}-278)/10)}$	Europe	Scheldt estuary	Regnier and Steefel (1999), Arndt et al. (2009) Volta et al. (2014)

Table B2. Continued.

k_{denit} , denitrification rate constant [$\mu\text{M C s}^{-1}$]				
2.60×10^{-5}	$k_{\text{denit}}(T) = k_{\text{denit,L}} \cdot 1.07^{(T-20)}$	Europe	Venice lagoon	Solidoro et al. (2005)
3.72×10^{-5}	–	Europe	Venice lagoon	Blauw et al. (2009)
3.69×10^{-4}	$k_{\text{denit}}(T) = k_{\text{denit,L}} \cdot 10^{((T_{\text{abs}}-278.15)/22.6)}$	Europe	Scheldt estuary	Regnier et al. (1997)
4.63×10^{-4}	$k_{\text{denit}}(T) = k_{\text{denit,L}} \cdot 2.75^{((T_{\text{abs}}-278)/10)}$	Europe	Scheldt estuary	Regnier and Steefel (1999) Arndt et al. (2009) Volta et al. (2014)
5.05×10^{-4}	$k_{\text{denit}}(T) = k_{\text{denit,L}} \cdot 1.08^{(T-20)}$	N. America	Satilla estuary	Zheng et al. (2004)
5.06×10^{-4}	$k_{\text{denit}}(T) = k_{\text{denit,L}} \cdot 2^{((T-15)/10)}$	Europe	Scheldt estuary	Hofmann et al. (2008)
6.41×10^{-4}	$k_{\text{denit}}(T) = k_{\text{denit,L}} \cdot 1.05^{(T-20)}$	Europe	Urdaibai estuary	Garcia et al. (2010)
7.77×10^{-3}	$k_{\text{denit}}(T) = k_{\text{denit,L}} \cdot \exp((T-10) \cdot \ln(1.65)/10)$	Europe	Scheldt estuary	Soetaert and Herman (1995)
9.07×10^{-3}	$k_{\text{denit}}(T) = k_{\text{denit,L}} \cdot 1.08^{(T-20)}$	Australia	Swan estuary	Robson and Hamilton (2004)
$5.22 \times 10^{-1*}$	$k_{\text{denit}}(T) = k_{\text{denit,L}} \cdot 2^{((T-15)/10)}$	Australia	Derwent estuary	Wild-Allen et al. (2009)
k_{nit} , nitrification rate constant [$\mu\text{MN s}^{-1}$]				
1.06×10^{-5}	–	N. America	Chesapeake Bay	HydroQual Inc. (1987) (via Lung and Paerl, 1988)
1.08×10^{-5}	–	N. America	Neuse estuary	Lung and Paerl (1988),
1.12×10^{-5}	–	N. America	James estuary	Lung (1986) (via Lung and Paerl, 1988)
1.16×10^{-5}	–	Europe	Venice lagoon	Blauw et al. (2009)
1.50×10^{-5}	–	N. America	Pamlico Sound	Lin et al. (2007)
1.60×10^{-5}	$k_{\text{nit}}(T) = k_{\text{nit,L}} \cdot 1.08^{(T-20)}$	Australia	Swan estuary	Robson and Hamilton (2004)
1.71×10^{-5}	$k_{\text{nit}}(T) = k_{\text{nit,L}} \cdot 1.07^{(T-20)}$	Europe	Venice lagoon	Solidoro et al. (2005)
1.93×10^{-5}	–	N. America	Potomac estuary	Thomann and Fitzpatrick (1982) (via Lung and Paerl, 1988)
2.67×10^{-5}	$k_{\text{nit}}(T) = k_{\text{nit,L}} \cdot 2^{((T-15)/10)}$	Australia	Derwent estuary	Wild-Allen et al. (2009)
2.79×10^{-5}	–	N. America	Potomac estuary	Thomann and Fitzpatrick (1982) (via Lung and Paerl, 1988)
3.20×10^{-5}	–	N. America	Cape Fear estuary	Lin et al. (2008)
3.37×10^{-5}	–	N. America	James estuary	Lung (1986) (via Lung and Paerl, 1988)
$5.51 \times 10^{-5**}$	$k_{\text{nit}}(T) = k_{\text{nit,L}} \cdot 1.08^{(T-20)}$	N. America	Satilla estuary	Zheng et al. (2004)
2.44×10^{-4}	$k_{\text{nit}}(T) = k_{\text{nit,L}} \cdot 2^{((T-15)/10)}$	Europe	Scheldt estuary	Hofmann et al. (2008)
4.64×10^{-4}	$k_{\text{nit}}(T) = k_{\text{nit,L}} \cdot \exp(-0.0045 \cdot (T-27)^2)$	N. America	Chesapeake Bay	Cerco and Cole (1994)
8.49×10^{-4}	$k_{\text{nit}}(T) = k_{\text{nit,L}} \cdot 5^{((T_{\text{abs}}-278.15)/10)}$	Europe	Scheldt estuary	Regnier et al. (1997) Regnier and Steefel (1999)
1.72×10^{-3}	$k_{\text{nit}}(T) = k_{\text{nit,L}} \cdot 5^{((T_{\text{abs}}-278)/10)}$	Europe	Scheldt estuary	Arndt et al. (2009) Volta et al. (2014)
2.17×10^{-3}	$k_{\text{nit}}(T) = k_{\text{nit,L}} \cdot \exp((T-10) \cdot \ln(3.37)/10)$	Europe	Scheldt estuary	Soetaert and Herman (1995)

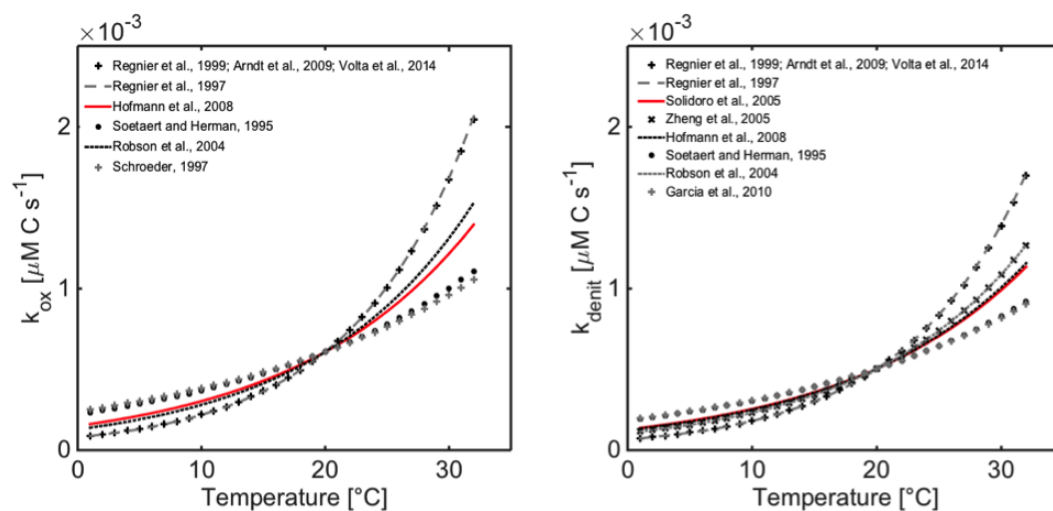


Figure B1. Temperature functions for aerobic degradation (k_{ox} , left panel) and denitrification (k_{denit} , right panel) rate constants as reported in the reviewed modeling applications (Table B2) for a reference T of 20 °C. Red lines indicate the T functions as used in the present study (Table 3). Note that only T functions associated with k_{ox} and k_{denit} values not recognized as outliers are displayed.

The Supplement related to this article is available online at doi:10.5194/hess-20-991-2016-supplement.

Acknowledgements. G. G. Laruelle is “Chargé de recherches du F.R.S.-FNRS” at the Université Libre de Bruxelles. S. Arndt acknowledges funding from the UK Natural Environmental Research Council (NE/I021322/1). The research leading to these results received funding from the European Union’s Horizon 2020 research and innovation program under Marie Skłodowska-Curie grant agreement no. 643052 (C-CASCADES project).

Edited by: A. D. Reeves

References

- Alongi, D. M.: Coastal Ecosystem Processes, in: CRC Mar. Sci. Ser., 1st Edn., edited by: Kennish, M. J. and Lutz, P. L., CRC Press, New York, 1998.
- Alpine, A. E. and Cloern, J. E.: Trophic interactions and direct physical effects control phytoplankton biomass and production in an estuary, *Limnol. Oceanogr.*, 37, 946–955, 1992.
- Andersson, A. J. and Mackenzie, F. T.: Shallow-water ocean: A source or sink of atmospheric CO₂?, *Front. Ecol. Environ.*, 2, 348–353, 2004.
- Andersson, A. J., Mackenzie, F. T., and Lerman, A.: Coastal ocean and carbonate systems in the high CO₂ world of the Anthropocene, *Am. J. Sci.*, 305, 875–918, 2005.
- Arndt, S. and Regnier, P.: A model for the benthic-pelagic coupling of silica in estuarine ecosystems: sensitivity analysis and system scale simulation, *Biogeosciences*, 4, 331–352, doi:10.5194/bg-4-331-2007, 2007.
- Arndt, S., Vanderborght, J. P., and Regnier, P.: Diatom growth response to physical forcing in a macrotidal estuary: Coupling hydrodynamics, sediment transport and biogeochemistry, *J. Geophys. Res.*, 112, C05045, doi:10.1029/2006JC003581, 2007.
- Arndt, S., Regnier, P., and Vanderborght, J. P.: Seasonally-resolved nutrient filtering capacities and export fluxes in a macrotidal estuary, *J. Mar. Syst.*, 78, 42–58, 2009.
- Arndt, S., Lacroix, G., Gypens, N., Regnier, P., and Lancelot, C.: Nutrient dynamics and phytoplankton development along an estuary-coastal zone continuum: A model study, *J. Mar. Syst.*, 84, 49–66, 2011a.
- Arndt, S., Regnier, P., Goddérès, Y., and Donnadiou, Y.: GEOCLIM *reloaded* (v 1.0): a new coupled earth system model for past climate change, *Geosci. Model Dev.*, 4, 451–481, doi:10.5194/gmd-4-451-2011, 2011b.
- Atlas, R., Hoffman, R. N., Ardizzone, J., Leidner, S. M., Jusem, J. C., Smith, D. K., and Gombos, D.: A cross-calibrated multiplatform ocean surface wind velocity product for meteorological and oceanographic applications, *B. Am. Meteorol. Soc.*, 92, 157–174, 2011.
- Baeyens, W., van Eck, B., Lambert, C., Wollast, R., and Goeyens, L.: General description of the Scheldt estuary, *Hydrobiologia*, 366, 1–14, 1998.
- Baklouti, M., Chevalier, C., Bouvy, M., Corbin, D., Pagano, M., Troussellier, M., and Arfi, R.: A study of plankton dynamics under osmotic stress in the Senegal River Estuary, West Africa, using a 3D mechanistic model, *Ecol. Model.*, 222, 2704–2721, 2011.
- Bauer, J. E., Cai, W.-J., Raymond, P. A., Bianchi, T. S., Hopkinson, C. S., and Regnier, P. A. G.: The changing carbon cycle of the coastal ocean, *Nature*, 504, 61–70, doi:10.1038/nature12857, 2013.
- Bianchi, T. S. (Ed.): *Biogeochemistry of estuaries*, first edition, Oxford University Press, New York, 2007.
- Billen, G., Somville, M., De Becker, E., and Servais, P.: A nitrogen budget of the Scheldt hydrographical basin, *Neth. J. Sea Res.*, 19, 223–230, 1985.
- Billen, G. and Garnier, J.: The Phison River plume: coastal eutrophication in response to change in land use and water management in the watershed, *Aquat. Microb. Ecol.*, 13, 3–17, 1997.
- Billen, G., Thieu, V., Garnier, J., and Silvestre, M.: Modelling the N cascade in regional waters: The case study of the Seine, Somme and Scheldt rivers, *Agr. Ecosyst. Environ.*, 133, 234–246, 2009.
- Blauw, A. N., Los, H. F. J., Bokhorst, M., and Erftemeijer, P. L. A.: GEM: a generic ecological model for estuaries and coastal waters, *Hydrobiologia*, 618, 175–198, 2009.
- Borges, A. V. and Abril, G.: Carbon Dioxide and Methane Dynamics in Estuaries, in: *Treatise on Estuarine and Coastal Science*, Volume 5: Biogeochemistry, edited by: Wolanski, E. and McLusky, D., Academic Press, Waltham, 119–161, 2011.
- Brock, T.: Calculating solar radiation for ecological studies, *Ecol. Model.*, 14, 1–19, 1981.
- Brzezinski, M. A.: The Si-C-N ratio of marine diatoms – Interspecific variability and the effect of some environmental variables, *J. Phycol.*, 21, 347–357, 1985.
- Bukaveckas, P. A. and Isenberg, W. N.: Loading, Transformation, and Retention of Nitrogen and Phosphorous in the Tidal Freshwater James River (Virginia), *Estuar. Coast.*, 36, 1219–1236, 2013.
- Caffrey, J. M.: Production, respiration and Net Ecosystem Metabolism in U.S. Estuaries, *Environ. Monit. Assess.*, 81, 207–219, 2003.
- Cai, W. J.: Estuarine and Coastal Ocean Carbon Paradox: CO₂ Sinks or Sites of Terrestrial Carbon Incineration, *Annu. Rev. Mar. Sci.*, 3, 123–145, 2011.
- Cai, W. J. and Wang, Y.: The chemistry, fluxes and sources of carbon dioxide in the estuarine waters of the Satilla and Altamaha Rivers, Georgia, *Limnol. Oceanogr.*, 43, 657–668, 1998.
- Canu, D. M., Solidoro, C., and Umgiesser, G.: Modelling the responses of the Lagoon of Venice ecosystem to variations in physical forcings, *Ecol. Model.*, 170, 265–289, 2003.
- Cerco, C. F.: Phytoplankton Kinetics in the Chesapeake Bay Eutrophication Model, *Water. Qual. Ecosyst. Model.*, 1, 5–49, 2000.
- Cerco, C. F. and Cole, T.: Three-dimensional eutrophication model of Chesapeake Bay, *J. Environ. Eng.*, 119, 1006–1025, 1994.
- Cerco, C. F. and Noel, M. R.: Process-based primary production modelling in Chesapeake Bay, *Mar. Ecol.-Prog. Ser.*, 282, 45–58, 2004.
- Chapelle, A., Lazure, P., and Menesguen, A.: Modelling Eutrophication Events in a Coastal Ecosystem. Sensitivity Analysis, *Estuar. Coast. Shelf S.*, 39, 529–548, 1994.
- Chapelle, A., Menesguen, A., Deslous-Paoli, J. M., Souchu, P., Mazouni, N., Vaquer, A., and Millet, B.: Modelling nitrogen, primary production and oxygen in a Mediterranean lagoon. Impact

- of oysters farming and inputs from the watershed, *Ecol. Model.*, 127, 161–181, 2000.
- Chen, C. T. A., Huang, T. H., Chen, Y. C., Bai, Y., He, X., and Kang, Y.: Air-sea exchanges of CO₂ in the world's coastal seas, *Biogeosciences*, 10, 6509–6544, doi:10.5194/bg-10-6509-2013, 2013.
- Crossland, C. J., Kremer, H. H., and Lindeboom, H. J. (Eds.): *Coastal Fluxes in the Anthropocene*, first edition, Springer, Berlin, 2005.
- Cugier, P., Billen, G., Guillaud, J. F., and Menesguen, A.: Modelling the eutrophication of the Seine Bight (France) under historical, present and future riverine nutrient loading, *J. Hydrol.*, 304, 381–396, 2005.
- Dalrymple, R. W., Zaitlin, B. A., and Boyd R.: Estuarine facies models: Conceptual basis and stratigraphic implications, *J. Sediment. Petrol.*, 62, 1130–1146, 1992.
- Datta-Gupta, A., Lake, L., Pope, G., Sepehrnoori, K., and King, M.: High-resolution monotonic schemes for reservoir fluid flow simulation, *In Situ*, 15, 289–317, 1991.
- Dauvin, J., Fisson, C., Garnier, J., Lafite, R., Ruellet, T., Billen, G., Deloffre, J., and Verney, R.: A report card and quality indicators for the Seine estuary: From scientific approach to operational tool, *Mar. Pollut. Bull.*, 57, 187–201, 2008.
- Davies, G. and Woodroffe, C. D.: Tidal estuary width convergence: Theory and form in North Australian estuaries, *Earth Surf. Proc. Land.*, 35, 737–749, 2010.
- Desmit, X., Vanderborght, J. P., Regnier, P., and Wollast, R.: Control of phytoplankton production by physical forcing in a strongly tidal, well-mixed estuary, *Biogeosciences*, 2, 205–218, doi:10.5194/bg-2-205-2005, 2005.
- Dickson, A.: Thermodynamics of the dissociation of boric acid in synthetic seawater from 273.15 to 318.15 K, *Deep-Sea Res. Pt. I*, 37, 755–766, 1990.
- Dürr, H. H., Laruelle, G. G., Van Kempen, C. M., Slomp, C. P., Maybeck, M., and Middelkoop, H.: World-wide typology of Near-shore Coastal Systems: Defining the Estuarine Filter of River Inputs to the Oceans, *Estuar. Coast.*, 34, 441–458, 2011.
- Ferreira, J. G., Duarte, P., and Ball, B.: Trophic capacity of Carlingford Lough for oyster culture – analysis by ecological modelling, *Aquat. Ecol.*, 31, 361–378, 1998.
- Follows, M. J., Ito, T., and Dutkiewicz, S.: On the solution of the carbonate chemistry system in ocean biogeochemistry models, *Ocean Model.*, 12, 290–301, 2006.
- Frankignoulle, M., Abril, G., Borges, A., Bourge, I., Canon, C., Delille, B., Libert, E., and Theate, J. M.: Carbon Dioxide Emission from European Estuaries, *Science*, 282, 434–436, 1998.
- Garcia, A., Juanes, J. A., Alvarez, C., Revilla, J. A., and Medina, R.: Assessment of the response of a shallow macrotidal estuary to changes in hydrological and wastewater inputs through numerical modelling, *Ecol. Model.*, 221, 1194–1208, 2010.
- Garnier, J., Billen, G., and Costa, M.: Seasonal succession of diatoms and Chlorophyceae in the drainage network of the Seine River: Observations and modeling, *Limnol. Oceanogr.*, 40, 750–765, 1995.
- Garnier, J., Servais, P., Billen, G., Akopian, M., and Brion, N.: Lower Seine River and Estuary (France) Carbon and Oxygen Budgets During Low Flow, *Estuaries*, 24, 964–976, 2001.
- Gattuso, J. P., Frankignoulle, M., and Wollast, R.: Carbon and Carbonate Metabolism in Coastal Aquatic System, *Annu. Rev. Ecol. Syst.*, 29, 405–434, 1998.
- Gaulke, A. K., Wetz, M. S., and Paerl, H. W.: Picophytoplankton: A major contributor to planktonic and primary production in a eutrophic river-dominated estuary, *Estuar. Coast. Shelf S.*, 90, 45–54, 2010.
- Geyer, W. R., Morris, J. T., Pahl, F. G., and Jay, D. A.: Interaction between physical processes and ecosystem structure: a comparative approach, in: *Estuarine Science: A Synthetic Approach to Research and Practice*, edited by: Hobbie, J. E., Island Press, Washington, D.C., 177–206, 2000.
- Gisen, J. I. A. and Savenije, H. H. G.: Estimating bankfull discharge and depth in ungauged estuaries, *Water Res. Res.*, 51, 2298–2316, doi:10.1002/2014WR016227, 2015.
- Gisen, J. I. A., Savenije, H. H. G., and Nijzink, R. C.: Revised predictive equations for salt intrusion modeling in estuaries, *Hydrol. Earth Syst. Sci.*, 19, 2791–2803, doi:10.5194/hess-19-2791-2015, 2015.
- Goñi, M. A., Teixeira, M. J., and Perkey, D. W.: Sources and distribution of organic matter in a river-dominated estuary (Winyah Bay, SC, USA), *Estuar. Coast. Shelf S.*, 57, 1023–1048, 2003.
- Griffin, S. L., Herzfeld, M., and Hamilton, D. P.: Modelling the impact of zooplankton grazing on phytoplankton biomass during a dinoflagellate bloom in the Swan River Estuary, Western Australia, *Ecol. Eng.*, 16, 373–394, 2001.
- Guillaud, J. F., Andrieux, F., and Ménesguen, A.: Biogeochemical modelling in the Bay of Seine (France): an improvement by introducing phosphorus in nutrient cycles, *J. Mar. Syst.*, 25, 369–386, 2000.
- Gypens, N., Delhez, E., Vanhoute-Brunier, A., Burton, S., Thieu, V., Passy, P., Liu, Y., Callens, J., Rousseau, V., and Lancelot, C.: Modelling phytoplankton succession and nutrient transfer along the Scheldt estuary (Belgium, The Netherlands), *J. Mar. Syst.*, 128, 89–105, 2013.
- Hartmann, J., Lauerwald, R., and Moosdorf, N.: A brief overview of the GLObal River Chemistry Database, GLORICH, *Proced. Earth Planet. Sci.*, 10, 23–27, 2014.
- Hartmann, J., Jansen, N., Dürr, H. H., Kempe, S., and Köhler, P.: Global CO₂-consumption by chemical weathering: What is the contribution of highly active weathering regions?, *Global Planet. Change*, 69, 185–194, doi:10.1016/j.gloplacha.2009.07.007, 2009.
- Hobbie, J. E. (Ed.): *Estuarine science: the key to progress in coastal ecological research*, in: *Estuarine Science: A Synthetic Approach to Research and Practice*, Island Press, Washington, D.C., 1–11, 2000.
- Hofmann, A. F., Soetaert, K., and Middelburg, J. J.: Present nitrogen and carbon dynamics in the Scheldt estuary using a novel 1-D model, *Biogeosciences*, 5, 981–1006, doi:10.5194/bg-5-981-2008, 2008.
- Horrigán, S. G., Montoya, J. P., McCarthy, J. J., Ducklow, H., Gericke, R., and Malone, T.: Nitrogenous Nutrient Transformations in the Spring and Fall in the Chesapeake Bay, *Estuar. Coast. Shelf S.*, 30, 369–391, 1990.
- Howland, R. J. M., Tappin, A. D., Uncles, R. J., Plummer, D. H., and Bloomer, N. J.: Distributions and seasonal variability of pH and alkalinity in the Tweed Estuary, UK, *Sci. Total Environ.*, 251–252, 125–138, 2000.

- Huret, M., Dadou, I., Dumas, F., Lazure, P., and Garçon, V.: Coupling physical and biogeochemical processes in the Rio de la Plata plume, *Cont. Shelf Res.*, 25, 629–653, 2005.
- HydroQual Inc.: Development of a coupled hydrodynamic/water quality model of eutrophication and anoxia processes of the Chesapeake Bay, Tech. Rep., US EPA, USA, 1987.
- IPCC Report: Climate Change 2013: The Physical Science Basis, in: Contribution of Working Group I to the Fifth Assessment Report of the Intergovernmental Panel on Climate Change, edited by: Stocker, T. F., Qin, D., Plattner, G.-K., Tignor, M., Allen, S. K., Boschung, J., Nauels, A., Xia, Y., Bex, V., and Midgley, P. M., Cambridge University Press, Cambridge, UK and New York, NY, USA, 2013.
- Jahnke, R. A.: The global ocean flux of particulate organic carbon: areal distribution and magnitude, *Global Biogeochem. Cy.*, 10, 71–88, 1996.
- Jay, D. A., Giese, B. S., and Sherwood, C. R.: Energetics and sedimentary processes in the Columbia River estuary, *Prog. Oceanogr.*, 25, 157–174, 1990.
- Jiang, I.-Q., Cai, W.-J., and Wang, Y.: A comparative study of carbon dioxide degassing in river- and marine-dominated estuaries, *Limnol. Oceanogr.*, 53, 2603–2651, 2008.
- Jonas, P. J. C. and Millward, G. E.: Metals and nutrients in the Severn Estuary and Bristol Channel: Contemporary inputs and distributions, *Mar. Pollut. Bull.*, 61, 52–67, 2010.
- Jones Jr., J. B., Stanley, E. H., and Mulholland, P. J.: Long-term decline in carbon dioxide supersaturation in rivers across the contiguous United States, *J. Geophys. Res. Lett.*, 30, 1495, doi:10.1029/2003GL017056, 2003.
- Kim, S. and Cerco, C. F.: Hydrodynamic and eutrophication model of the Chester River estuary and the Eastern Bay estuary, Tech. Rep., US Army Engineer Research and Development Center, USA, 2003.
- Kroeze, C. and Seitzinger, S. P.: Nitrogen inputs to rivers, estuaries and continental shelves and related nitrous oxide emissions in 1990 and 2050: a global model, *Nutr. Cycl. Agroecosys.*, 52, 195–212, 1998.
- Lancelot, C., Spitz, Y., Gypens, N., Ruddick, K., Becquevort, S., Rousseau, V., Lacroix, G., and Billen, G.: Modelling diatom and Phaeocystis blooms and nutrient cycles in the Southern Bight of the North Sea: the MIRO model, *Mar. Ecol.-Prog. Ser.*, 289, 63–78, 2005.
- Lanzoni, S. and Seminara, G.: On tide propagation in convergent estuaries, *J. Geophys. Res.-Oceans*, 103, 30793–30812, 1998.
- Laruelle, G. G.: Quantifying nutrient cycling and retention in coastal waters at the global scale, PhD thesis, Universiteit Utrecht, Utrecht, the Netherlands, 2009.
- Laruelle, G. G., Regnier, P., Ragueneau, O., Kempa, M., Moriceau, B., Ni Longphuir, S., Leynaert, A., Thouzeau, G., and Chauvaud, L.: Benthic-pelagic coupling and the seasonal silica cycle in the Bay of Brest (France): new insights from a coupled physical-biological model, *Mar. Ecol.-Prog. Ser.*, 385, 15–32, 2009.
- Laruelle, G. G., Dürr, H. H., Slomp, C. P., and Borges, A. V.: Evaluation of sinks and sources of CO₂ in the global coastal ocean using a spatially-explicit typology of estuaries and continental shelves, *Geophys. Res. Lett.*, 37, L15607, doi:10.1029/2010GL043691, 2010.
- Laruelle, G. G., Dürr, H. H., Lauerwald, R., Hartmann, J., Slomp, C. P., Goossens, N., and Regnier, P. A. G.: Global multi-scale segmentation of continental and coastal waters from the watersheds to the continental margins, *Hydrol. Earth Syst. Sci.*, 17, 2029–2051, doi:10.5194/hess-17-2029-2013, 2013.
- Laruelle, G. G., Lauerwald, R., Pfeil, B., and Regnier, P.: Regionalized budget of the CO₂ exchange at the air-water interface in continental shelf seas, *Global Biogeochem. Cy.*, 28, 1199–1214, doi:10.1002/2014GB004832, 2014.
- Lauerwald, R., Laruelle, G. G., Hartmann, J., Ciais, P., and Regnier, P. A. G.: Spatial patterns in CO₂ evasion from the global river network, *Global Biogeochem. Cy.*, 29, 534–554, doi:10.1002/2014GB004941, 2015.
- Lee, D. I., Parl, C. K., and Cho, H. S.: Ecological modeling for water quality management of Kwangyang Bay, Korea, *J. Environ. Manage.*, 74, 327–337, 2005.
- Leonard, B.: Third-Order Upwinding as a Rational Basis for Computational Fluid Dynamics, in: *Computational Techniques and Applications: CTAC-83*, edited by: Noye, J. and Fletcher, C. A. J., Elsevier, North-Holland, 1984.
- Le Pape, O. and Ménesguen, A.: Hydrodynamic prevention of eutrophication in the Bay of Brest (France), a modelling approach, *J. Mar. Syst.*, 12, 171–186, 1997.
- Le Pape, O., Jean, F., and Ménesguen, A.: Pelagic and benthic trophic chain coupling in a semi-enclosed coastal system, the Bay of Brest (France): a modelling approach, *Mar. Ecol.-Prog. Ser.*, 189, 135–147, 1999.
- Lin, J., Xie, L., Pietrafesa, L. J., Ramus, J. S., and Paerl, H. W.: Water Quality Gradients across Albemarle-Pamlico Estuarine System: Seasonal Variations and Model Applications, *J. Coast. Res.*, 23, 213–229, 2007.
- Lin, J., Xie, L., Pietrafesa, L. J., Xu, H., Woods, W., Mallin, M. A., and Durako, M. J.: Water quality responses to simulated flow and nutrient reductions in the Cape Fear River Estuary and adjacent coastal region, North Carolina, *Ecol. Model.*, 212, 200–217, 2008.
- Lung, W. S.: Assessing phosphorous control in the James River basin, *J. Environ. Eng.-ASCE*, 112, 44–60, 1986.
- Lung, W. S. and Paerl, H. W.: Modeling blue-green algal blooms in the lower Neuse river, *Water Resour.*, 22, 895–905, 1988.
- Macedo, M. F. and Duarte, P.: Phytoplankton production modelling in three marine ecosystems – static versus dynamic approach, *Ecol. Model.*, 190, 299–316, 2006.
- Mackenzie, F. T., Lerman, A., and Andersson, A. J.: Past and present of sediment and carbon biogeochemical cycling models, *Biogeosciences*, 1, 11–32, doi:10.5194/bg-1-11-2004, 2004.
- Mackenzie, F. T., Andersson, A. J., Lerman, A., and Ver, L. M.: Boundary exchanges in the global costal margin: implications for the organic and inorganic carbon cycles, in: *The sea*, edited by: Robinson, A. R. and Brink, K. H., Harvard University Press, Cambridge, 193–225, 2005.
- Mackenzie, F. T., Lerman, A., and DeCarlo, E. H.: Coupled C, N, P and O biogeochemical cycling at the land-ocean interface, in: *Treatise in Coastal and Estuarine Science, Volume 5: Biogeochemistry*, edited by: Wolanski, E. and McLusky, D., Elsevier, Academic Press, Waltham, 317–342, 2011.
- Margvelashvili, N., Robson, B., Sakov, P., Webster, I. T., Parslow, J., Herzfeld, M., and Andrewartha, J.: Numerical modelling of hydrodynamics, sediment transport and biogeochemistry in the

- Fitzroy Estuary, Tech. Rep. 9, Cooperative Research Centre for Coastal Zone Estuary and Waterway Management, Australia, 2003.
- Mateus, M., Vaz, N., and Neves, R.: A process-oriented model of pelagic biogeochemistry for marine systems. Part II: Application to a mesotidal estuary, *J. Mar. Syst.*, 94, 90–101, 2012.
- Mayorga, E., Seitzinger, S. P., Harrison, J. A., Dumont, E., Beusen, A. H. W., Bouwman, A. F., Fekete, B. M., Kroeze, C., and Van Drecht, G.: Global nutrient export from WaterSheds 2 (NEWS 2): model development and implementation, *Environ. Model. Softw.*, 25, 837–853, 2010.
- Mendenhall, W., Beaver, R., and Beaver, B. (Eds.): *Introduction to Probability and Statistics*, fourteenth edition, Brooks/Cole, Boston, 2013.
- Meybeck, M.: Carbon, nitrogen, and phosphorous transport by world rivers, *Am. J. Sci.*, 282, 401–450, 1982.
- Moss, R. H., Edmonds, J. A., Hibbard, K. A., Manning, M. R., Rose, S. K., van Vuuren, D. P., Carter, T. R., Emori, S., Kainuma, M., Kram, T., Meehl, G. A., Mitchell, J. F. B., Nakicenovic, N., Riahi, K., Smith, S. J., Stouffer, R. J., Thomson, A. M., Weyant, J. P., and Wilbanks, T. J.: The next generation of scenarios for climate change research and assessment, *Nature*, 463, 747–756, 2010.
- Nihoul, J. C. J. and Roday, F.: Modèles d'estuaires partiellement stratifiés, in: *Projet Mer*, Vol. 10, Service de la Programmation Scientifique, Bruxelles, Belgium, 71–98, 1976.
- Nixon, S. W., Ammerman, J. W., Atkinson, L. P., Berounsky, V. M., Billen, G., Boicourt, W. C., Boynton, W. R., Church, T. M., Ditoro, D. M., Elmgren, R., Garber, J. H., Giblin, A. E., Jahnke, R. A., Owens, N. J. P., Pilson, M. E. Q., and Seitzinger, S. P.: The fate of nitrogen and phosphorus at the land-sea margin of the North Atlantic Ocean, *Biogeochemistry*, 35, 141–180, 1996.
- Odum, H. T.: Primary Production in Flowing Waters, *Limnol. Oceanogr.*, 1, 102–117, 1956.
- Park, K., Jung, H. S., Kim, H. S., and Ahn, S. M.: Three-dimensional hydrodynamic-eutrophication model (HEM-3D): application to Kwang-Yang Bay, Korea, *Mar. Environ. Res.*, 60, 171–193, 2005.
- Peterson, D. H. and Festa, J. F.: Numerical Simulation of Phytoplankton Productivity in Partially Mixed Estuaries, *Estuar. Coast. Shelf S.*, 19, 563–589, 1984.
- Pethick, J. S. (Ed.): *An introduction to coastal geomorphology*, 1st Edn., Arnold E., London, 1984.
- Pethick, J. S.: Saltmarsh geomorphology, in: *Saltmarshes: morphodynamics, conservation and engineering significance*, edited by: Allen, J. R. L. and Pye, K., Cambridge University Press, Cambridge, 1992.
- Press, W. H., Teukolsky, S. A., Vetterling, W. T., and Flannery, B. P. (Eds.): *Numerical Recipes in C: The Art of Scientific Programming*, second edition, Cambridge University Press, USA, 1992.
- Pritchard, D. W.: The Equations of Mass Continuity and Salt Continuity in Estuaries, *J. Mar. Res.*, 15, 33–42, 1958.
- Pritchard, D. W.: What is an estuary: physical viewpoint, in: *Estuaries*, edited by: Lauf, G. H., American Association for the Advancement of Science (AAAS), Publ. No. 83, Washington, DC, 3–5, 1967.
- Raymond, P. A., Oh, N.-H., Turner, R. E., and Broussard, W.: Anthropogenically enhanced fluxes of water and carbon from the Mississippi River, *Nature*, 451, 449–452, 2008.
- Redfield, A. C., Ketchum, B. H., and Richards, F. A.: The influence of organisms on the composition of seawater, in: *The Sea*, Vol. 2, edited by: Hill, M. N., Interscience, New York, 26–77, 1963.
- Regnier, P. and Steefel, C. I.: A high resolution estimate of the inorganic nitrogen flux from the Scheldt estuary to the coastal North Sea during a nitrogen-limited algal bloom, spring 1995, *Geochim. Cosmochim. Acta*, 63, 1359–1374, 1999.
- Regnier, P., Wollast, R., and Steefel, C. I.: Long-term fluxes of reactive species in macrotidal estuaries: Estimates from a fully transient, multicomponent reaction-transport model, *Mar. Chem.*, 58, 127–145, 1997.
- Regnier, P., Mouchet, A., Wollast, R., and Roday, F.: A discussion of methods for estimating residual fluxes in strong tidal estuaries, *Cont. Shelf Res.*, 18, 1543–1571, 1998.
- Regnier, P., Friedlingstein, P., Ciais, P., Mackenzie, F. T., Gruber, N., Janssens, I. A., Laruelle, G. G., Lauerwald, R., Luyssaert, S., Andersson, A. J., Arndt, S., Arnosti, C., Borges, A. V., Dale, A. W., Gallego-Sala, A., Goddérès, Y., Goossens, N., Hartmann, J., Heinze, C., Ilyina, T., Joos, F., LaRowe, D. E., Leifeld, J., Meysman, F. J. R., Munhoven, G., Raymond, P. A., Spahni, R., Suntharalingam, P., and Thullner, M.: Anthropogenic perturbation of the carbon fluxes from land to ocean, *Nat. Geosci.*, 6, 597–607, doi:10.1038/ngeo1830, 2013a.
- Regnier, P., Arndt, S., Goossens, N., Volta, C., Laruelle, G. G., Lauerwald, R., and Hartmann, J.: Modelling Estuarine Biogeochemical Dynamics: From the Local to the Global Scale, *Aquat. Geochem.*, 19, 591–626, 2013b.
- Robson, B. J. and Hamilton, D. P.: Three-dimensional modelling of a *Microcystis* bloom event in the Swan River estuary, Western Australia, *Ecol. Model.*, 174, 203–222, 2004.
- Ruddick, K., Park, Y., and Nechad, B.: MERIS imagery of Belgian coastal waters: mapping of suspended particulate matter and chlorophyll-*a*, in: *Meris Users Workshop*, vol. SP-549, ESA Special Publication, Frascati, 2003.
- Savenije, H. H. G.: A one-dimensional model for salinity intrusion in alluvial estuaries, *J. Hydrol.*, 85, 87–109, 1986.
- Savenije, H. H. G.: *Rapid Assessment Technique for Salt Intrusion in Alluvial Estuaries*, PhD Thesis, IHE Report Series 27, International Institute for Infrastructure, Hydraulics and Environment, Delft, the Netherlands, 1992.
- Savenije, H. H. G.: A simple analytical expression to describe tidal damping or amplification, *J. Hydrol.*, 243, 205–215, 2001.
- Savenije, H. H. G. (Ed.): *Salinity and Tides in Alluvial Estuaries*, 1st Edn., Elsevier, Amsterdam, 2005.
- Savenije, H. H. G. (Ed.): *Salinity and Tides in Alluvial Estuaries*, 2nd Edn., available at: <http://salinityandtides.com> (last access: 8 March 2015), 2012.
- Schroeder, F.: Water quality in the Elbe estuary: Significance of different processes for the oxygen deficit at Hamburg, *Environ. Model. Assess.*, 2, 73–82, 1997.
- SeaWiFS: <http://oceancolor.gsfc.nasa.gov>, last access: 14 November 2014.
- Seitzinger, S. P.: Denitrification in freshwater and coastal marine ecosystems: Ecological and geochemical significance, *Limnol. Oceanogr.*, 33, 702–724, 1988.
- Seitzinger, S. P., Mayorga, E., Bouwman, A. F., Kroeze, C., Beusen, A. H. W., Billen, G., Van Drecht, G., Dumont, E., Fekete, B. M., Garnier, J., and Harrison, J. A.: Global river nutrient export: A

- scenario analysis of past and future trends, *Global Biogeochem. Cy.*, 24, GBOA08, doi:10.1029/2009GB003587, 2010.
- Sharp, J. H., Yoshiyama, K., Parker, A. E., Schwartz, M. C., Curless, S. E., Beauregard, A. Y., Ossolinski, J. E., and Davis, A. R.: A Biogeochemical View of the Estuarine Eutrophication: Seasonal and Spatial Trends and Correlations in the Delaware Estuary, *Estuar. Coast.*, 32, 1023–1043, 2009.
- Simmons, H. B.: Some effects of inland discharge on estuarine hydraulics, *Proc. Am. Soc. Civ. Eng.-ASCE*, 81, 792, 1955.
- Soetaert, K. and Herman, P. M. J.: Nitrogen dynamics in the Westerschelde estuary (S.W. Netherlands) estimated by means of the ecosystem model MOSES, *Hydrobiologia*, 311, 225–246, 1995.
- Soetaert, K., Herman, P. M. J., and Kromkamp, J.: Living in the twilight: estimating net phytoplankton growth in the Westerschelde estuary (The Netherlands) by means of an ecosystem model (MOSES), *J. Plankton Res.*, 16, 1277–1301, 1994.
- Solidoro, C., Pastres, R., and Cossarini, G.: Nitrogen and plankton dynamics in the lagoon of Venice, *Ecol. Model.*, 184, 103–124, 2005.
- Thomann, R. and Fitzpatrick, J.: Calibration and verification of a mathematical model of the eutrophication of the Potomac Estuary, *Tech. Rep.*, HydroQual Inc., Mahwah, 1982.
- Toffolon, M., Vignoli, G., and Tubino, M.: Relevant parameters and finite amplitude effects in estuarine hydrodynamics, *J. Geophys. Res.*, 111, C10014, doi:10.1029/2005JC003104, 2006.
- Trancoso, A. R., Saraiva, S., Fernandes, L., Pina, P., and Neves, R.: Modelling macroalgae using a 3D hydrodynamic-ecological model in a shallow, temperate estuary, *Ecol. Model.*, 187, 232–246, 2005.
- Vanderborght, J. P., Wollast, R., Loijens, M., and Regnier P.: Application of a transport-reactive model to the estimation of biogas fluxes in the Scheldt estuary, *Biogeochemistry*, 59, 207–237, 2002.
- Vanderborght, J. P., Folmer, I., Aguilera, D. R., Uhrenholdt, T., and Regnier, P.: Reactive-transport modelling of a river-estuarine-coastal zone system: application to the Scheldt estuary, *Mar. Chem.* 106, 92–110, 2007.
- Volta, C., Arndt, S., Savenije, H. H. G., Laruelle, G. G., and Regnier, P.: C-GEM (v 1.0): a new, cost-efficient biogeochemical model for estuaries and its application to a funnel-shaped system, *Geosci. Model Dev.*, 7, 1271–1295, doi:10.5194/gmd-7-1271-2014, 2014.
- Voss, M., Dippner, J. W., Humborg, C., Hurdler, J., Korth, F., Neumann, T., Schernewski, G., and Venohr, M.: History and scenarios of future development of Baltic Sea eutrophication, *Estuar. Coast. Shelf S.*, 92, 307–322, 2011.
- Wells, J. T.: Tide-Dominated Estuaries and Tidal Rivers, in: *Geomorphology and Sedimentology of Estuaries*, Development in Sedimentology 53, edited by: Perillo, G. M. E., Elsevier Science, New York, 179–205, 1995.
- Wild-Allen, K., Skerratt, J., Rizwi, F., and Parslow, J.: Derwent Estuary Biogeochemical Model: Technical Report, *Tech. Rep.*, CSIRO Mar. Atmos. Res., CSIRO, Canberra, 2009.
- Winterwerp, J. C.: On the flocculation and settling velocity of estuarine mud, *Cont. Shelf Res.*, 22, 1339–1360, 2002.
- World Ocean Atlas: <http://www.nodc.noaa.gov/OC5/indprod.html>, last access: 9 May 2014.
- Wright, L. D., Coleman, J. M., and Thom, B. G. Processes of channel development in a high-tide-range environment: Cambridge Gulf-Ord river delta. Western Australia, *J. Geol.*, 81, 15–41, 1973.
- Zeebe, R. E. and Wolf-Gladrow, D. (Eds.): *CO₂ in seawater: equilibrium, kinetics, isotopes*, Elsevier, Amsterdam, 2001.
- Zemlys, P., Erturk, A., and Razinkovas, A.: 2D finite element ecological model for the Curonian lagoon, *Hydrobiologia*, 611, 167–179, 2008.
- Zheng, L., Chen, C., and Zhang, F.: Development of water quality model in the Satilla River Estuary, Georgia, *Ecol. Model.*, 178, 457–482, 2004.